EPJ A
Hadrons and Nuclei

EPJ.org
your physics journal

Eur. Phys. J. A (2018) **54**: 87 DOI 10.1140/epja/i2018-12521-7

Revisiting the residual temperature distribution in prompt neutron emission in fission

A. Tudora, F.-J. Hambsch and V. Tobosaru

Società Italiana di Fisica

Springer

Eur. Phys. J. A (2018) **54**: 87
DOI 10.1140/epja/i2018-12521-7

THE EUROPEAN PHYSICAL JOURNAL A

Regular Article – Theoretical Physics

Revisiting the residual temperature distribution in prompt neutron emission in fission

A. Tudora[1,a], F.-J. Hambsch[2], and V. Tobosaru[1]

[1] University of Bucharest, Faculty of Physics, 405 Atomistilor Str., POB MG-11, RO-77125, Bucharest, Magurele, Romania
[2] European Commission, Joint Research Centre, Directorate G – Nuclear Safety and Security, Unit G2, Retiese weg 111, B-2440, Geel, Belgium

Received: 14 February 2018 / Revised: 21 April 2018
Published online: 29 May 2018

Communicated by F. Gulminelli

Abstract. A new triangular form of the residual temperature distribution $P(T)$, entering the prompt emission models in which the sequential emission is globally taken into account (*e.g.*, the Los Alamos model of Madland and Nix with subsequent improvements and the Point-by-Point model), is proposed. A deterministic treatment of the successive emission of prompt neutrons, which is based on recursive equations of the residual temperatures, was developed. This modeling was validated by the good description of many and different experimental data of prompt emission (*e.g.*, $\overline{\nu}(A)$, $\langle\nu\rangle$(TKE), $\langle\varepsilon\rangle(A)$, $\langle\varepsilon\rangle$(TKE), $\overline{E}_\gamma(A)$, etc.) and the good agreement with the results of other prompt emission models. To see a possible systematic behaviour of $P(T)$ as a function of energy and fissioning nucleus, the deterministic treatment of sequential emission was applied to 11 nuclei undergoing fission (spontaneously or induced by thermal and fast neutrons with energies up to the threshold of the second chance fission) for which reliable experimental fission fragment distributions $Y(A, \mathrm{TKE})$ exist. The shapes of all $P(T)$ distributions for the light and heavy fragment groups and for all fragments resulting from this modeling can be approximated with a triangular form. To make possible the use of this form into the prompt emission models with a global treatment of sequential emission, a connection between the average residual temperature $\langle\mathrm{Tr}\rangle$ and the temperature of initial fragments $\langle\mathrm{Ti}\rangle$ is needed. An important finding of this study concerns the ratio $\langle\mathrm{Tr}\rangle/\langle\mathrm{Ti}\rangle$, which is ≈ 0.6 for all studied fissioning systems. This result allows to obtain a new triangular form of $P(T)$ defined only as a function of initial temperature, which is applicable to any fissioning system at any energy, in the frame of prompt emission models with a global treatment of sequential emission.

1 Introduction

The main objective of the study described in this paper was to determine a new triangular form of the residual temperature distribution $P(T)$ which is used in the Los Alamos (LA) model [1–3] and the prompt emission model Point-by-Point (PbP) ([3,4], and references therein).

In these models the sequential emission is globally taken into account by the residual temperature distribution $P(T)$. *I.e.*, the prompt neutron spectrum in the center-of-mass frame corresponding to an initial fragment is given by the integral of an evaporation spectrum at a given residual temperature $\varphi(\varepsilon, T)$ over the $P(T)$ distribution. The residual temperature distribution, which was used in both the LA and PbP models, has a triangular form with a sharp high temperature cut-off and its first order momentum is expressed as a function of initial fragment temperature by $\langle T\rangle = (2/3)T_i$ [1].

In this study the residual temperature distribution is obtained in the frame of a deterministic treatment of the successive emission of prompt neutrons, which is based on the recursive equations of residual temperatures. Different approaches concerning the compound nucleus cross-section of the inverse process of successive neutron evaporation and the level density parameters of initial and residual fragments are analyzed in order to solve these successive residual temperature equations.

In this modeling of sequential emission the fragmentation range is deterministically constructed as in the PbP treatment. For each initial fragment $\{A, Z\}$ at a given total kinetic energy (TKE) covering the fragmentation range, an equation of residual temperature is solved for each sequence of successive neutron emission. Then different quantities characterizing the residual nucleus and the prompt emission are obtained for each emission sequence indexed k, where k is running over the number of prompt neutrons emitted successively (or the number of residual fragments) corresponding to an initial fragment at a given TKE.

[a] e-mail: anabellatudora@hotmail.com

Using the multiple distributions of initial fragments $Y(A, Z, \mathrm{TKE})$, different distributions can be obtained. These could be distributions of the residual temperature and the residual energy and of the average neutron energy in the center-of-mass frame, corresponding to the emission of each neutron as well as the sum of these distributions following the emission of all neutrons from the light and heavy fragment groups and from all fragments.

Different quantities generically labeled $q(A, Z, \mathrm{TKE})$ corresponding to an initial fragment at a TKE value (*e.g.*, the prompt neutron multiplicity $\nu(A, Z, \mathrm{TKE})$, the average center-of-mass energy of prompt neutrons $\langle\varepsilon\rangle(A, Z, \mathrm{TKE})$, the prompt neutron spectrum in the center-of-mass frame $\varphi(\varepsilon, A, Z, \mathrm{TKE})$, the average prompt γ-ray energy of all γ-rays $E\gamma(A, Z, \mathrm{TKE})$, etc.) can be obtained by averaging the respective quantities corresponding to each sequence, $q_k(A, Z, \mathrm{TKE})$, over the number of sequences (*i.e.*, the number of emitted neutrons).

In order to see a possible systematic behaviour of the residual temperature distribution as a function of energy and fissioning nucleus, the deterministic treatment of sequential emission based on the successive equations of residual temperature was applied to 11 fissioning nuclei for which reliable experimental fission fragment distributions exist. The nuclei investigated were: $^{235}\mathrm{U}(\mathrm{n_{th}}, \mathrm{f})$, $^{252}\mathrm{Cf(SF)}$, $^{239}\mathrm{Pu}(\mathrm{n_{th}}, \mathrm{f})$ with $Y(A, \mathrm{TKE})$ distributions measured at JRC-Geel [5–7], $^{236,238,240,242,244}\mathrm{Pu(SF)}$ for which the $Y(A, \mathrm{TKE})$ data of Dematté [8] were used, $^{237}\mathrm{Np}(\mathrm{n}, \mathrm{f})$, $^{238}\mathrm{U}(\mathrm{n}, \mathrm{f})$ and $^{234}\mathrm{U}(\mathrm{n}, \mathrm{f})$ for which $Y(A, \mathrm{TKE})$ distributions were measured at incident neutron energies (En) up to about 5 MeV at JRC-Geel, too [9–11].

The good agreement of different prompt emission quantities obtained from this sequential emission treatment (*e.g.*, $\overline{\nu}(A)$, $\langle\nu\rangle(\mathrm{TKE})$, $\langle\varepsilon\rangle(A)$, $\langle\varepsilon\rangle(\mathrm{TKE})$, $\overline{E}_\gamma(A)$, $P(\nu)$, etc.) with the experimental data and the results of other prompt emission models (*e.g.*, PbP, FIFRELIN, etc.) validates this deterministic modeling of successive emission of prompt neutrons.

The shapes of residual temperature distributions for the light and heavy fragment groups and for all fragments resulting from this modeling can be approximated with a triangular form with a moderately broad cut-off at high temperatures. In order to make possible the use of this form into prompt emission models with a global treatment of sequential emission, a connection between the average residual temperature and the temperature of initial fragments (before the emission of prompt neutrons) is needed.

A very interesting finding of this study concerns the ratio of the average residual temperature to the initial temperature, which is ≈ 0.6 for all studied fissioning systems (including the nuclei fissioning at different incident neutron energies ranging up to about 5 MeV). This result, *i.e.* $\langle T\rangle = 0.6\langle T_i\rangle$, together with the replacement of the moderately broad high temperature cut-off of the triangular $P(T)$ form by a sharp cut-off, allows to obtain a new triangular form of $P(T)$ which can be applied to any fissioning nucleus at any energy.

The present paper is organized in the following sections: the present introduction, a second section devoted to the successive equations of residual temperature on which the sequential emission treatment is based, together with approximations regarding the compound nucleus cross-section of the inverse process and the level density parameter of initial and residual fragments which are used to solve these equations. A third section contains the distributions of different quantities (*e.g.*, residual temperature, residual energy and average center-of mass energy of prompt neutrons) following the successive emission of each neutron. Section 4 contains the validation of sequential emission calculations by comparison with the experimental data and the results of other prompt emission models. Section 5 includes the residual temperature distributions obtained from the present sequential emission treatment and the new triangular form resulting from this study. Results of the PbP model, in which the new $P(T)$ form is included, are exemplified in sect. 6. The last section summarizes the conclusions of this study.

2 Equation of residual temperature following the successive emission of each prompt neutron

For a given fissioning nucleus the initial fragmentation range is constructed as in the PbP treatment (ref. [4] and references therein), *i.e.* the mass number A of initial fragments (before to emit prompt neutrons) covers a large range, from symmetric fission up to a very asymmetric split, with a step of one mass unit. For each A three charge numbers Z are taken as the nearest integer values above and below the most probable charge which is taken as the unchanged charge distribution (UCD) corrected with the charge polarization: $Zp(A) = Z_{UCD}(A) + \Delta Z(A)$. For a part of the fissioning nuclei studied in this work (*i.e.*, $^{235}\mathrm{U}(\mathrm{n_{th}}, \mathrm{f})$, $^{252}\mathrm{Cf(SF)}$, $^{239}\mathrm{Pu}(\mathrm{n_{th}}, \mathrm{f})$) the charge polarization $\Delta Z(A)$ and the root-mean-square rms(A) of the Gaussian isobaric charge distribution, centered on $Zp(A)$, are given by the Zp model of Wahl [12]. For the other fissioning nuclei ($^{236-244}\mathrm{Pu(SF)}$, $^{234,238}\mathrm{U}(\mathrm{n}, \mathrm{f})$ and $^{237}\mathrm{Np(n,f)}$) constant values of ΔZ and rms are taken for all fragments, *i.e.* the mean values $\Delta Z = |0.5|$ (with plus sign for light fragments and minus sign for heavy fragments) and rms = 0.6. For each fragmentation a large TKE range is taken (*e.g.*, from 100 to 200 MeV) with a step size of 5 MeV.

For each initial fragment A, Z at each TKE value the successive emission of prompt neutrons is taken into account as follows.

If a first prompt neutron ($k = 1$) can be emitted from an initial fragment $\{Z, A\}$ at a given TKE value then the excitation energy of the first residual nucleus $\{Z, A-1\}$ can be expressed as $\overline{E_r}^{(1)} = E^* - S_n^{(0)} - \langle\varepsilon\rangle_1$, where E^* is the excitation energy of the initial fragment resulting from the partition of the total excitation energy of fully accelerated complementary fragments (TXE) based on modeling at scission [4,13,14], $S_n^{(0)}$ is the neutron separation energy from the initial fragment and $\langle\varepsilon\rangle_1$ is the average center-of-mass energy of the first emitted neutron. Considering the

level densities of fragments (initial and residuals) in the Fermi gas regime (*i.e.*, $\overline{E} = a\overline{T}^2$ where a is the level density parameter and T the nuclear temperature), an equation for the nuclear temperature of the first residual nucleus can be written as $E^* - S_n^{(0)} - \langle\varepsilon\rangle_1 = a_1 T_1^2$. If a second neutron ($k = 2$) can be emitted (by evaporation from the first residual nucleus) then $\overline{E_r}^{(1)} - S_n^{(1)} - \langle\varepsilon\rangle_2 = a_2 T_2^2$, and the successive neutron emission continues up to a number of $k_{\max}$ prompt neutrons, which is limited by the last residual nucleus $\{Z, A - k_{\max}\}$ with an excitation energy less than its neutron separation energy.

Consequently the temperature of the k-th residual nucleus $\{Z, A-k\}$ following the emission of the k-th prompt neutron is the solution of the following equation:

$$\overline{E_r}^{(k-1)} - S_n^{(k-1)} - \langle\varepsilon\rangle_k = a_k T_k^2, \tag{1}$$

in which $\overline{E_r}^{(k-1)}$ and $S_n^{(k-1)}$ are the average excitation energy and the neutron separation energy of the precursor, $\langle\varepsilon\rangle_k$ is the average center-of-mass energy of the k-th emitted neutron, a_k and T_k are the level density parameter and the nuclear temperature of the k-th residual nucleus.

To solve these successive equations of residual temperatures the following aspects must be taken into account:

- the average prompt neutron energy in the center-of-mass frame $\langle\varepsilon\rangle_k$ expressed as a function of the residual temperature T_k and
- non energy dependent level density parameters of initial and residual fragments.

2.1 Average prompt neutron energy in the center-of-mass frame as a function of residual temperature

The center-of-mass energy spectrum of emitted prompt neutrons is given by the statistical model, *i.e.* $\varphi(\varepsilon) = \text{const}\,\varepsilon\sigma_c(\varepsilon)\rho(E^* - S_n - \varepsilon)$ in which $\sigma_c(\varepsilon)$ is the compound nucleus cross-section of the inverse process of neutron evaporation from fragments (*i.e.*, formation of a compound nucleus by an incident neutron of energy ε) and ρ is the nuclear level density. Note that the statistical model is more justified in the application to fission fragments than to most other nuclear reactions when a direct interaction of an incident particle is involved.

Considering the fragments as a degenerate Fermi gas (with the entropy $S = \ln\rho$), the level density can be expressed as $\rho(E^* - S_n - \varepsilon) \cong \text{const}\exp(-\varepsilon/\sqrt{\langle E_r\rangle/a})$ if $|\langle\varepsilon\rangle - \varepsilon| \ll \langle E_r\rangle$. This leads to the center-of-mass energy distribution of prompt neutrons usually expressed by the well-known Weisskopf evaporation spectrum

$$\varphi(\varepsilon, T) = K(T)\varepsilon\sigma_c(\varepsilon)\exp(-\varepsilon/T),$$
$$K(T) = \left(\int_0^\infty \varepsilon\sigma_c(\varepsilon)\exp(-\varepsilon/T)\mathrm{d}\varepsilon\right)^{-1}, \tag{2}$$

in which T is the nuclear temperature of the residual nucleus and $K(T)$ is the normalization constant. The first order momentum of this spectrum is calculated as

$$\langle\varepsilon\rangle(T) = K(T)\int_0^\infty \varepsilon^2\sigma_c(\varepsilon)\exp(-\varepsilon/T)\mathrm{d}\varepsilon. \tag{3}$$

In many modelings of prompt emission based on the Weisskopf evaporation spectrum (*e.g.*, PbP, FIFRELIN and others) the compound nucleus cross-section of the inverse process $\sigma_c(\varepsilon)$ is provided by optical model calculations with optical potential parameterizations appropriate for nuclei appearing as fission fragments (*e.g.*, Becchetti-Greenlees, Koning-Delaroche, etc. taken from RIPL3 [15]). In this case $\langle\varepsilon\rangle$ is obtained by the numerical integration of eq. (3). The use of such a numerical $\sigma_c(\varepsilon)$ from optical model calculations complicates very much the computational solution of the residual temperature equations (1).

The simplest approximation is to consider a near constant $\sigma_c(\varepsilon)$. In this case the spectrum of eq. (2) becomes $\varphi(\varepsilon, T) = \frac{1}{T^2}\varepsilon\exp(-\varepsilon/T)$ and the average energy is $\langle\varepsilon\rangle(T) = 2T$. The successive equations of residual temperature (1) become

$$\overline{E_r}^{(k-1)} - S_n^{(k-1)} - 2T_k = a_k T_k^2, \tag{4}$$

with the following simple analytical solutions for the residual temperature:

$$T_k = \frac{1}{a_k}\left(\sqrt{1 + \left(\overline{E_r}^{(k-1)} - S_n^{(k-1)}\right)} - 1\right). \tag{5}$$

Another approximation is to consider an analytical expression of $\sigma_c(\varepsilon)$ obtained by considering $\sigma_c(\varepsilon)$ as a sum of a constant term σ_0 and an s-wave term $\sigma_s(\varepsilon)$ which depends on $1/\sqrt{\varepsilon}$ according to ref. [16]. *I.e.*, $\sigma_0 = \pi R^2$ with $R = r_0 A^{1/3}$ (in which r_0 is the reduced radius) and $\sigma_s(\varepsilon) = (\pi/k^2)T_0 = S_0(\pi\hbar)^2/m\sqrt{\varepsilon}$ (where $k = \sqrt{2m\varepsilon}/\hbar$ is the wave number and $T_0 = 2\pi\sqrt{\varepsilon}S_0$ the transmission coefficient of the s-wave neutron). S_0 is the s-wave neutron strength function of a fission fragment with the mass number A and m is the neutron mass. Consequently $\sigma_c(\varepsilon)$ can be expressed as

$$\sigma_c(\varepsilon) = \sigma_0\left(1 + \frac{\alpha}{\sqrt{\varepsilon}}\right), \tag{6}$$

with $\alpha = (\hbar^2/mr_0^2)S_0/A^{2/3}$ depending on the mass number and the s-wave neutron strength function of each residual nucleus. With $\sigma_c(\varepsilon)$ given by eq. (6) the prompt neutron spectrum in the center-of-mass frame of eq. (2) and the average prompt neutron energy of eq. (3) become

$$\varphi(\varepsilon, T) = \frac{\varepsilon + \alpha\sqrt{\varepsilon}}{T^{3/2}(\sqrt{T} + \alpha\sqrt{\pi}/2)}\exp(-\varepsilon/T), \tag{7}$$

$$\langle\varepsilon\rangle(T) = \frac{T(2\sqrt{T} + (3\sqrt{\pi}/4)\alpha)}{\sqrt{T} + (\sqrt{\pi}/2)\alpha}. \tag{8}$$

The $\sigma_c(\varepsilon)$ approximation of eq. (6) leads to the following transcendent equations of residual temperatures:

$$\overline{E_r}^{(k-1)} - S_n^{(k-1)} - \frac{T_k(2\sqrt{T_k} + (3\sqrt{\pi}/4)\alpha_k)}{\sqrt{T_k} + (\sqrt{\pi}/2)\alpha_k} = a_k T_k^2, \tag{9}$$

which can be numerically solved.

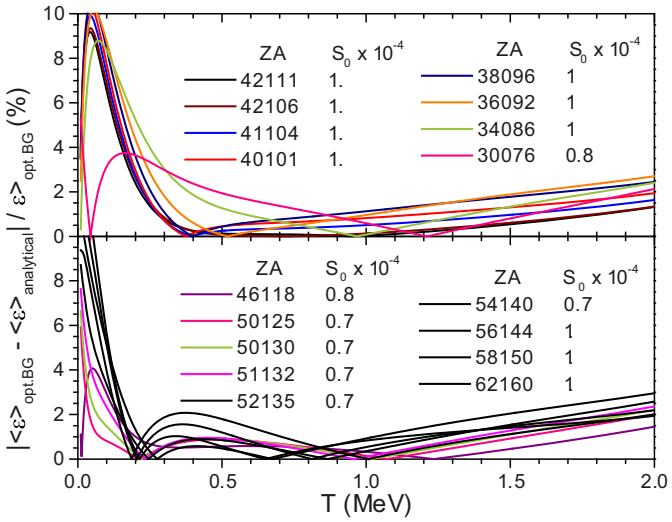

Fig. 1. Deviations of $\langle\varepsilon\rangle(T)$ based on the analytical $\sigma_c(\varepsilon)$ expression of eq. (6) from $\langle\varepsilon\rangle(T)$ based on numerical $\sigma_c(\varepsilon)$ provided by optical model calculations (with the Becchetti-Greenlees parameterization) exemplified for ten fragmentations of ^{235}U(n, f) (the light fragments in the upper part and the complementary heavy fragments in the lower part).

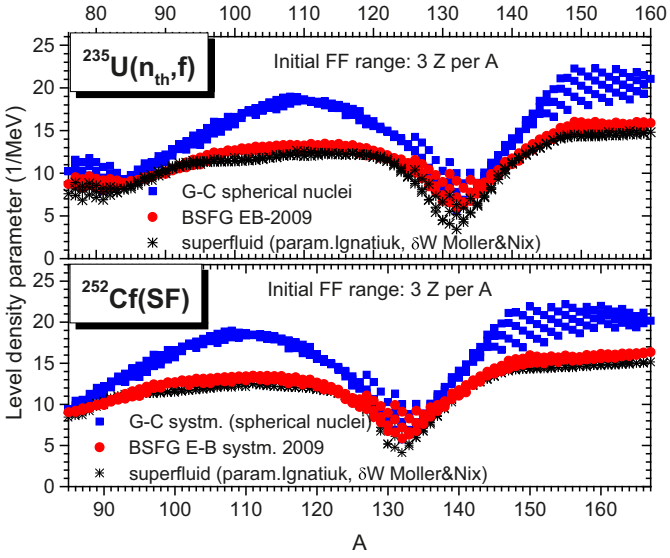

Fig. 2. Level density parameters of initial fragments of ^{235}U(n_{th}, f) (upper part) and ^{252}Cf(SF) (lower part) provided by the super-fluid model (black stars), the Egidy-Bucurescu systematic for the BSFG model (red circles) and the Gilbert-Cameron systematic (blue squares).

In order to see if $\langle\varepsilon\rangle(T)$ of eq. (8) based on $\sigma_c(\varepsilon)$ of eq. (6) can approximate the average prompt neutron energies of eq. (3) based on numerical $\sigma_c(\varepsilon)$ provided by optical model calculation, the following study was made.

Calculations of $\langle\varepsilon\rangle(T)$ according to eq. (8) were done for nuclei with mass numbers covering the usual A-range of fission fragments (*e.g.*, from 76 to 160) at temperature values ranging from 0.01 MeV to 2 MeV (with a step size of 0.001 MeV). For each mass number the calculations were done for average s-wave strength functions $\langle S_0\rangle$ with values ranging from 0.7×10^{-4} to 1.1×10^{-4} (with a step size of 0.1×10^{-4}) and the reduced radius was taken $r_0 = 1.2$ fm. The resulting $\langle\varepsilon\rangle(T)$ were compared with the ones obtained by numerical integration of eq. (3) at T values also ranging from 0.01 MeV to 2 MeV (with a step size of 0.001 MeV). The numerical $\sigma_c(\varepsilon)$ were provided by optical model calculations with the parameterization of Becchetti-Greenlees [15] for nuclei with A ranging from 76 to 160 and the charge number Z taken as the nearest integer of the most probable charge associated to the fissioning nucleus ^{236}U.

The deviations of $\langle\varepsilon\rangle(T)$ given by eq. (8) from $\langle\varepsilon\rangle(T)$ based on $\sigma_c(\varepsilon)$ provided by optical model calculations, obtained as

$$deviation(T) = \frac{|\langle\varepsilon\rangle(T)_{optBG} - \langle\varepsilon\rangle(T)_{analyt.}|}{\langle\varepsilon\rangle(T)_{optBG}}, \qquad (10)$$

are illustrated in fig. 1 for ten fragment pairs covering the fragmentation range of ^{235}U(n, f), the light fragments in the upper part and the complementary heavy fragments in the lower part. The s-wave strength function values of each nucleus (indicated as $ZA = 1000Z + A$) are given in the figure legend, too.

As it can be seen for T values ranging from 0.2 MeV to 2 MeV (which are typical values of the temperatures of residual nuclei following the sequential emission of prompt neutrons) the deviations are below 4%. This verification supports the use of the $\sigma_c(\varepsilon)$ approximation of eq. (6) in the successive equations of residual temperatures.

The use of a constant σ_c leads to deviations from $\langle\varepsilon\rangle$ based on $\sigma_c(\varepsilon)$ provided by optical model calculations which vary by about 13–14% at low T values (of about 0.2 MeV) up to about 7–8% at high T values (near 2 MeV).

Note, in the sequential emission calculations of this work, s-wave neutron strength functions as a function of A based on the $\langle S_0\rangle$ data from RIPL3 [17] were used.

2.2 Non energy-dependent level density parameters of fragments

In many models of prompt emission the level density parameter of the fragments is energy-dependent, being calculated in the frame of the super-fluid model of Ignatiuk [18] with different prescriptions concerning the shell corrections (δW) and the parameterizations of the damping of shell effects (γ) and the asymptotic level density parameter ($\tilde{a}$).

The non energy-dependent level density parameters provided by two systematics, *i.e.* of Gilbert and Cameron (GC) [19] and of von Egidy and Bucurescu (EB-2009) for the back-shift Fermi gas (BSFG) model [20], were compared with the energy-dependent level density parameters of the super-fluid model with shell corrections of Möller and Nix [21] and the γ and $\tilde{a}$ parameterizations of Ignatiuk [18]. In fig. 2 this comparison is done for the level

density parameters of initial fragments as a function of A, for the fissioning nuclei ^{235}U(n_{th}, f) (upper part) and ^{252}Cf(SF) (lower part). The level density parameters of the super-fluid model are plotted with black stars, those of the Gilbert-Cameron systematic with blue squares and of the Egidy-Bucurescu systematic for the BSFG model with red circles. As it can be seen the non energy-dependent level density parameters of the Egidy-Bucurescu systematic for the BSFG model are close to the ones of the super-fluid model over the entire fragment range, except for heavy fragments with A around 130 (for which large negative shell corrections exist due to the magic shells $N = 82$ and $Z = 50$). The level density parameters of the GC systematic are significantly higher than the ones of the super-fluid model and the EB-2009 systematic for the BSFG model.

The residual energies entering the successive transcendent equations of residual temperature are distributed over a range going up to about 20–30 MeV. The super-fluid level density parameters as a function of energy, calculated in this energy range for many nuclei appearing as residual fragments, were compared with the non energy-dependent level density parameters given by the EB-2009 systematic for the BSFG model.

For a large number of residual nuclei with A outside the range 125–135 the differences between the level density parameters of the super-fluid model [18] and the constant values of the EB-2009 systematic for BSFG [20] are of about 5–6%.

In the case of nuclei with A around 130, especially at lower energies (below 5 MeV) the super-fluid level density parameters are with 30–40% lower than those of BSFG. At higher energies the differences become less than 10%, in the majority of cases being less than 5%.

Consequently for initial and residual fragments with A outside the range 125–135 the non energy-dependent level density parameters of the EB-2009 systematic for the BSFG model can approximate well the energy-dependent level density parameters of the super-fluid model. In the case of nuclei with A in the range 125–135 the level density parameters provided by the super-fluid model at low energies are significantly lower than the constant values of the EB-2009 systematic for the BSFG model. This fact affects the average center-of-mass energy of prompt neutrons $\langle\varepsilon\rangle$ of residual nuclei with low excitation energies (less than 5 MeV) for which $\langle\varepsilon\rangle$ is very low. For this reason, the sequential emission results of $\langle\varepsilon\rangle$ as a function of A (given with blue symbols in the upper part of fig. 16) overestimate the experimental data and the results of other prompt emission models at A around 130.

Taking into account that

i) the recursive equations of residual temperature (1), (4), (9) can be solved only when the level density parameters are non energy-dependent and
ii) for a great part of initial and residual fragments (except the ones with A in the range 125–135 at low excitation energies) the level density parameters of the EB-2009 systematic for the BSFG model can approximate the energy-dependent level density parameters of the super-fluid model,

the level density parameters provided by the EB-2009 systematic for the BSFG model are used, together with $\sigma_c(\varepsilon)$ expressed by eq. (6), in the sequential emission calculations of all fissioning nuclei studied in this work. Calculations with other prescriptions, *i.e.* a constant σ_c and level density parameters given by the Gilbert-Cameron systematic for spherical nuclei, are also performed for a part of fissioning nuclei, in order to investigate possible differences in different distributions and prompt emission quantities.

The solution of the successive equations of residual temperature provides detailed quantities characterizing the residual fragments and the sequential neutron emission associated to each initial fragment at each TKE, appearing with the probability expressed by the fragment distribution $Y(A, Z, \mathrm{TKE})$. These quantities are the residual temperature and residual energy following the successive emission of each neutron $T_k(A, Z, \mathrm{TKE})$, ${E_r}^{(k)}(A, Z, \mathrm{TKE})$, the average center-of-mass energy and spectrum of each neutron emitted sequentially $\langle\varepsilon\rangle_k(A, Z, \mathrm{TKE})$ and $\varphi_k(\varepsilon, A, Z, \mathrm{TKE})$ with k going from 1 to the number of emission sequences $k_{\max}(A, Z, \mathrm{TKE})$ (*i.e.*, the number of emitted prompt neutrons from an initial fragment $\{Z, A\}$ at a given TKE value). For simplicity these quantities are generically labeled as $q_k(A, Z, \mathrm{TKE})$. Note that the neutron separation energy ${S_n}^{(k)}$ and the level density parameter a_k entering the successive equations of residual temperature (given by eq. (1), or (4), or (9)) are referring to the nuclei $\{Z, A-k\}$ (with $k = 0$ denoting the initial fragment).

The multiple $Y(A, Z, \mathrm{TKE})$ distributions are taken as a product of an isobaric charge distribution $p(Z, A)$ (which is a Gaussian centered on the most probable charge $Zp(A)$) and an experimental $Y(A, \mathrm{TKE})$ distribution (as mentioned in refs. [3,4] and references therein).

3 Distributions of different quantities following the successive emission of each neutron

The distributions of different quantities following the successive emission of each neutron (indexed k) are exemplified in figs. 3 and 4 as follows.

In fig. 3 the residual temperature distributions following the emission of the first (red), second (blue), third (green), 4th (wine), 5th neutron (dark yellow), etc. from light fragments (left part) and heavy fragments (right part) are plotted as histograms for ^{235}U(n_{th}, f) (upper part) and ^{252}Cf(SF) (lower part). The average values $\langle T_k\rangle$ of these distributions are also given in each frame. It can be seen that the residual temperature distributions following the successive emission of the first, second and third neutron exhibit almost triangular shapes with a moderately broad cut-off at high temperatures.

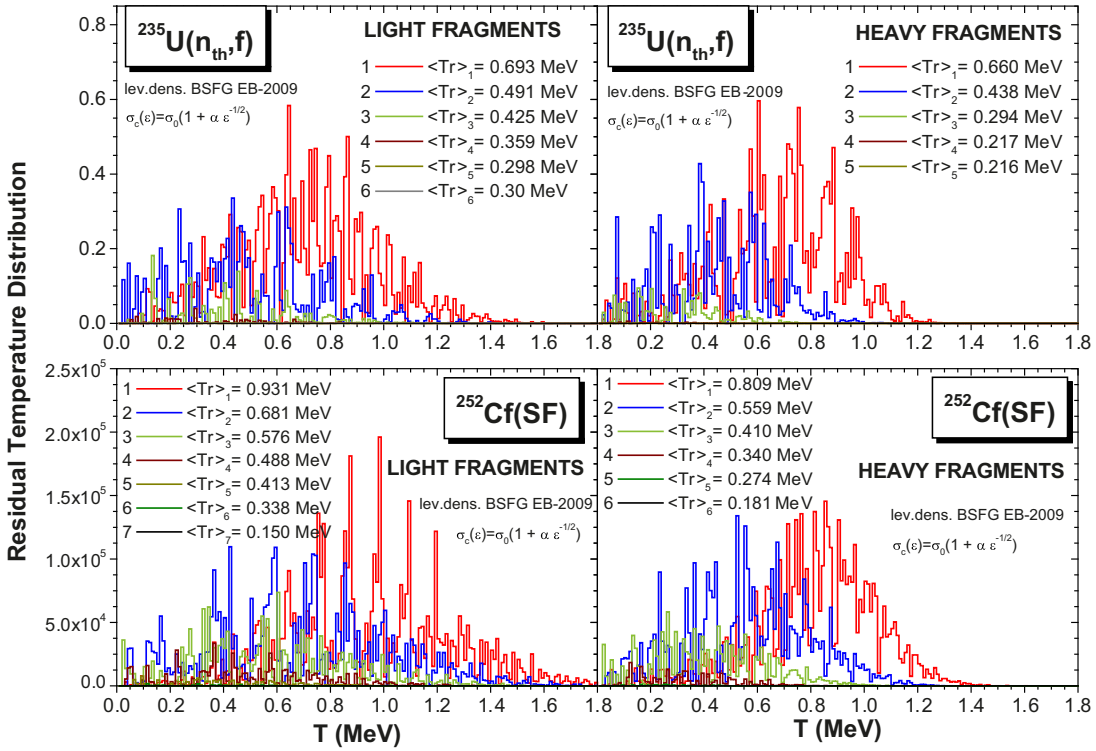

Fig. 3. Residual temperature distributions following the successive emission of the first (red), second (blue), third (green), 4th (wine) 5th neutron (dark yellow), etc. from light fragments (left part) and heavy fragments (right part) of the fissioning nuclei ^{235}U(n$_{\rm th}$, f) (upper part) and ^{252}Cf(SF) (lower part). Note that the distributions are not normalized, consequently the labels of vertical axes are arbitrary numbers depending on the statistical significance of the underlying experimental distributions $Y(A, \mathrm{TKE})$.

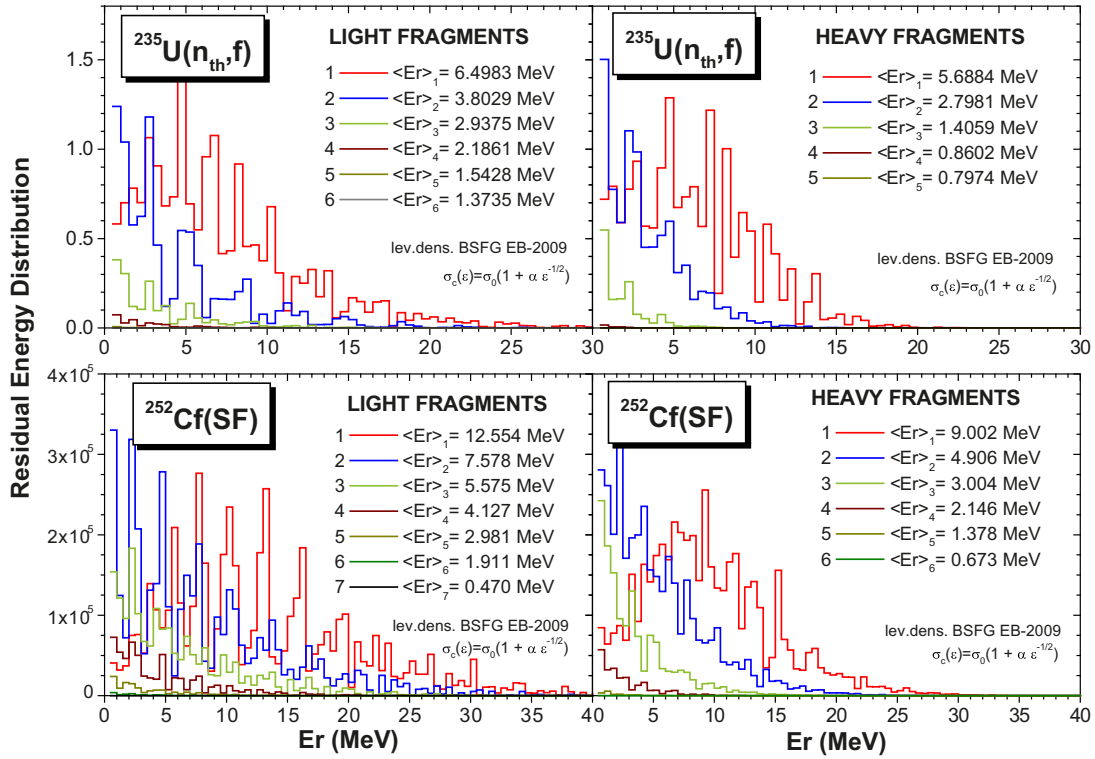

Fig. 4. Residual energy distributions following the successive emission of each neutron from the light fragments (left part) and heavy fragments (right part) of ^{235}U(n$_{\rm th}$, f) and ^{252}Cf(SF). Note that the distributions are not normalized, consequently the labels of vertical axes are arbitrary numbers depending on the statistical significance of the underlying experimental distributions $Y(A, \mathrm{TKE})$.

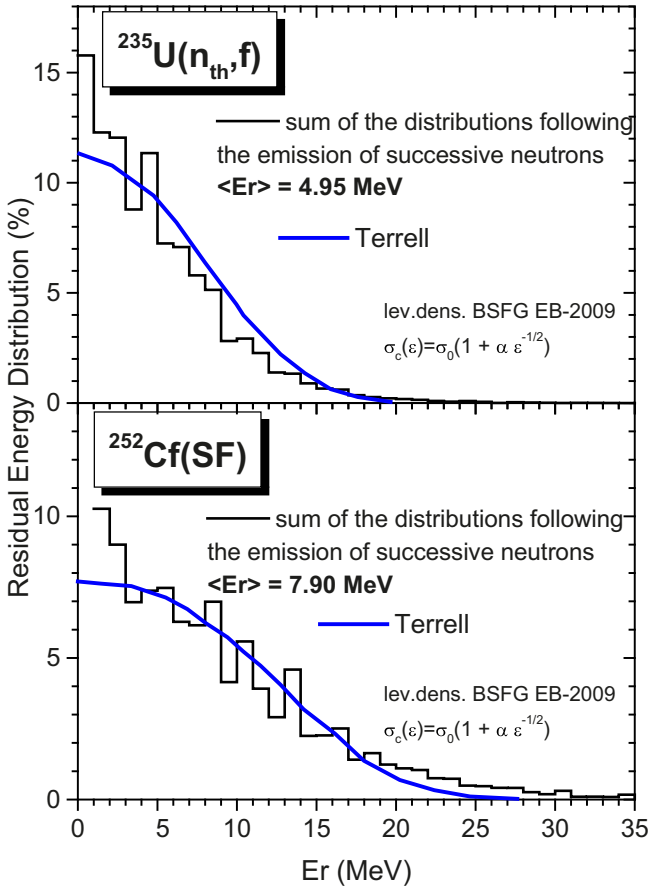

Fig. 5. Sum of residual energy distributions following the successive emission of all neutrons from all fragments (histograms plotted with black lines) of ^{235}U(n$_{\rm th}$, f) (upper part) and ^{252}Cf(SF) (lower part) in comparison with the results of Terrell (blue lines).

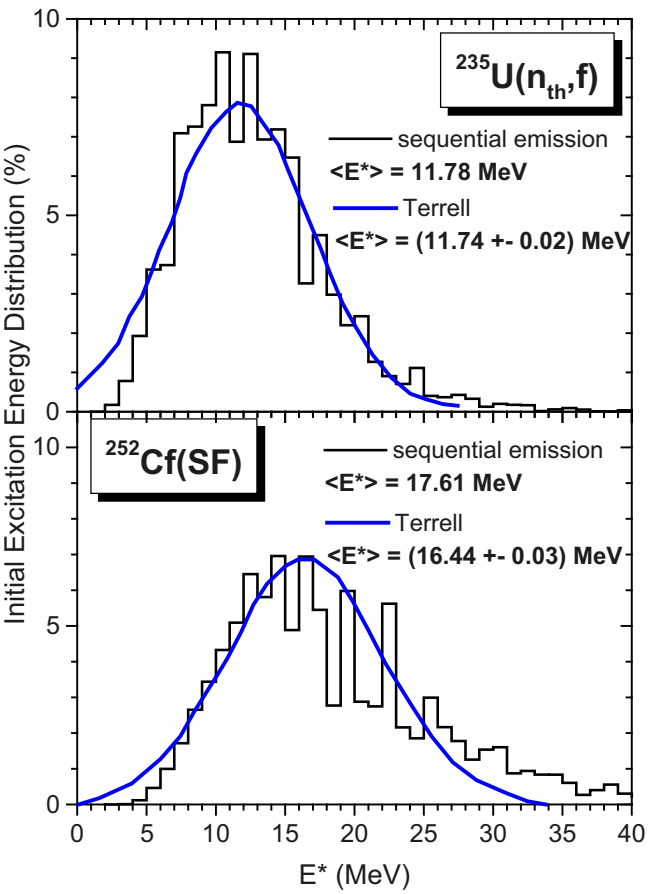

Fig. 6. Initial excitation energy distributions of ^{235}U(n$_{\rm th}$, f) (upper part) and ^{252}Cf(SF) (lower part) from the TXE partition based on modeling at scission (histograms plotted with black lines) and the results of Terrell (blue lines).

The residual energy distributions following the successive emission of the first, second, third, 4th, 5th neutron, etc. from the light and heavy fragments of ^{235}U(n$_{\rm th}$, f) and ^{252}Cf(SF) are plotted as histograms in fig. 4 using the same colors as in fig. 3. The average values $\langle E_r{}^{(k)} \rangle$ of these distributions are given in each frame, too.

The sum of residual energy distributions following the emission of each neutron from all fragments is plotted with a black line in fig. 5, for ^{235}U(n$_{\rm th}$, f) in the upper part and ^{252}Cf(SF) in the lower part. As it can be seen the present results are in good agreement with the residual energy distributions of Terrell [22] (blue lines).

Note, in ref. [22] the residual energy distributions for ^{235}U(n$_{\rm th}$, f) and ^{252}Cf(SF) were obtained from the distributions of initial excitation energies taken as Gaussian functions with average values and root-mean-squares depending on the average number of prompt neutrons and an excitation energy per nucleon of about 6.7 MeV. These distributions are plotted with blue lines in fig. 6. The present distributions of the excitation energy of initial fragments, which are obtained from the TXE partition based on modeling at scission (described in refs. [3,4] and references therein) are also plotted in fig. 6 as histograms with black lines. The agreement of the present initial excitation energy distributions based on modeling at scission with the ones of Terrell based on experimental observation, is very good.

The sum of the residual temperature distributions following the successive emission of all neutrons from the light and heavy fragments and from all fragments of all studied fissioning systems are given in sect. 5.

The average residual temperature and residual energy following the successive emission of each neutron as well as the average center-of-mass energy of each emitted neutron are plotted as a function of the initial fragment mass in fig. 7. They were obtained by averaging the quantities corresponding to the sequential emission of each neutron from an initial fragment over the distributions $Y(A, Z, \mathrm{TKE})$, *i.e.*

$$\overline{q}_k(A) = \sum_{Z,\mathrm{TKE}} q_k(A, Z, \mathrm{TKE}) \times Y(A, Z, \mathrm{TKE}) \Big/ \sum_{Z,\mathrm{TKE}} Y(A, Z, \mathrm{TKE}), \quad (11)$$

in which $q_k(A, Z, \mathrm{TKE})$ denotes $T_k(A, Z, \mathrm{TKE})$, $Er_k(A, Z, \mathrm{TKE})$ and $\langle \varepsilon \rangle_k(A, Z, \mathrm{TKE})$ and $\overline{q}_k(A)$ are the quantities plotted in fig. 7.

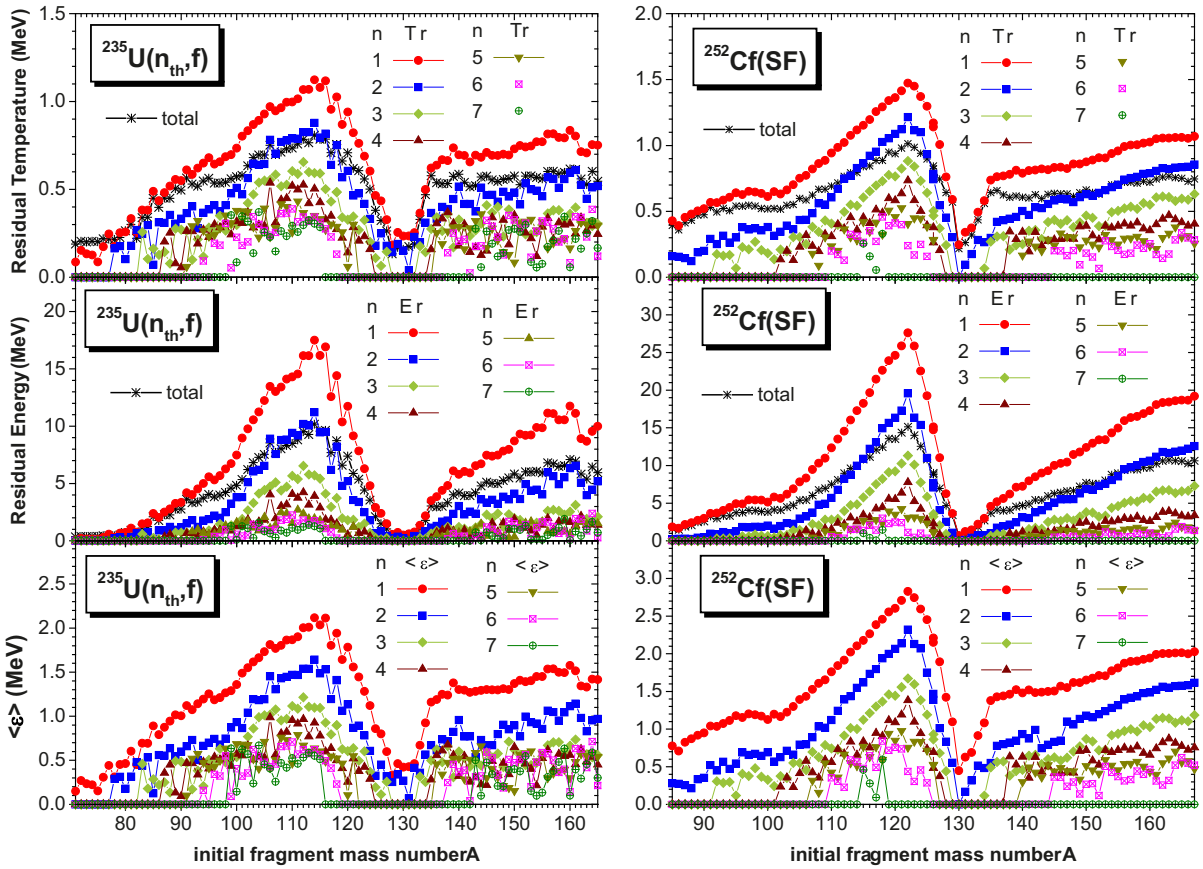

Fig. 7. The average residual temperature (upper part) and residual energy (middle) following the successive emission of each prompt neutron and the average center-of-mass energy of each emitted neutron (lower part) as a function of initial fragment mass exemplified for ^{235}U(n$_{\rm th}$, f) (left part) and ^{252}Cf(SF) (right part).

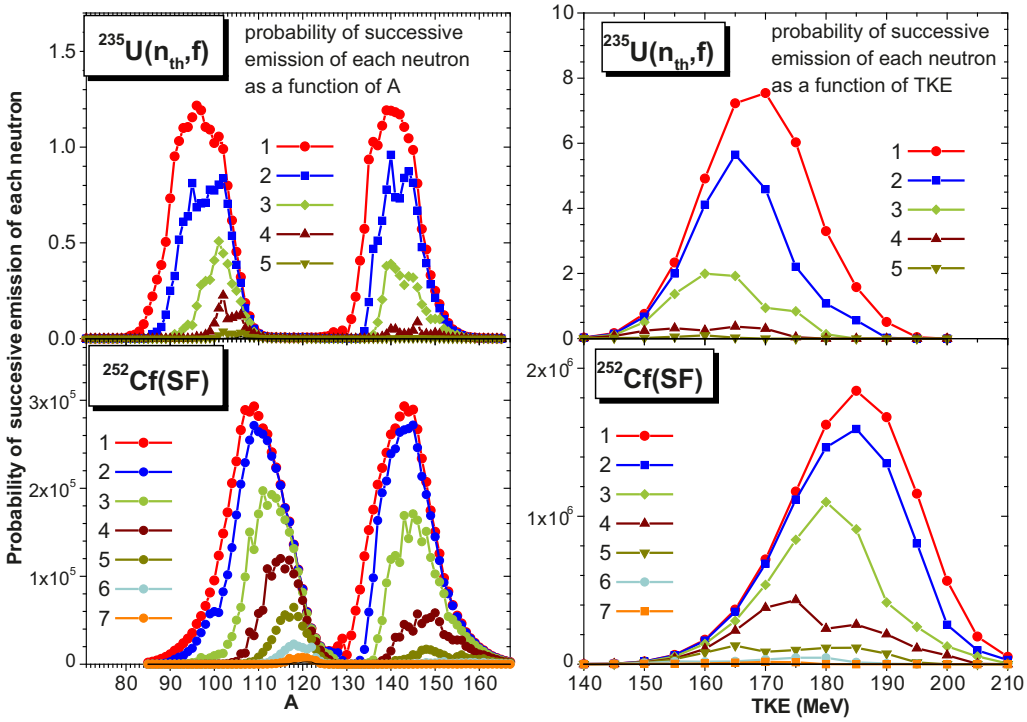

Fig. 8. Probability of emission of each prompt neutron as a function of initial fragment mass A (left part) and as a function of TKE (right part) exemplified for ^{235}U(n$_{\rm th}$, f) (upper part) and ^{252}Cf(SF) (lower part).

The sawtooth shape of these quantities corresponding to the first (red circles), second (blue squares) and third (green diamonds) emitted neutron is clearly visible. It can be also seen that the successive emission of more than 3 neutrons (*i.e.*, $k = 4, 5, 6$, etc.) is not possible for all initial fragment masses.

In fig. 8 the probability of emission of each prompt neutron as a function of initial fragment mass (left part) and as a function of TKE (right part) is illustrated for two fissioning nuclei, ^{235}U(n_{th}, f) and ^{252}Cf(SF). In the case of probabilities as a function of A it can be observed that the left humps for the third and 4th emitted neutron (green and wine symbols) are visibly higher than the corresponding right humps, *i.e.* the probability to emit sequentially three and four neutrons is higher for the light fragment group than for the heavy fragment group. The light and heavy fragment groups emit sequentially one and two neutrons (red and blue humps, respectively) with almost the same probability. This is not surprising because it is well known that for fissioning systems at low energy the average initial excitation energy of the light fragment group is higher than that of the heavy fragment group and also the average number of prompt neutrons emitted by the light fragment group is higher than the average number of neutrons emitted by the heavy fragment group.

4 Validation of sequential emission calculation by comparison with experimental data and results of other prompt emission models

To obtain the multi-parametric matrices of different quantities associated to an initial fragment at a given TKE, with probability $Y(A, Z, \mathrm{TKE})$, the sequential emission results are averaged over the number of sequences corresponding to the respective initial fragment, *i.e.*

$$\overline{q}(A, Z, \mathrm{TKE}) = \frac{1}{k_{\max}(A, Z, \mathrm{TKE})} \sum_{k=1}^{k_{\max}} q_k(A, Z, \mathrm{TKE}). \tag{12}$$

By averaging the quantities $\overline{q}(A, Z, \mathrm{TKE})$ given by eq. (12) in different ways over the $Y(A, Z, \mathrm{TKE})$ distributions (as mentioned in ref. [4] and references therein), different average prompt emission quantities are obtained, *e.g.* $\overline{q}(A)$ (by summing over Z and TKE), $\overline{q}(A, \mathrm{TKE})$ (by summing over Z), $\langle q \rangle(\mathrm{TKE})$ (by summing over A and Z), etc.

To validate this deterministic treatment of sequential emission, the average quantities mentioned above are compared with existing experimental data (*e.g.*, of $\overline{\nu}(A)$, $\langle \nu \rangle(\mathrm{TKE})$, $\langle \varepsilon \rangle(A)$, etc.). Examples of such comparisons are given in the next figures as follows.

One of the most significant comparisons concerns the average prompt neutron multiplicity as a function of initial fragment mass A, especially because this quantity is very sensitive to the TXE partition. Another comparison concerns the systematic behaviour of the experimental ratio

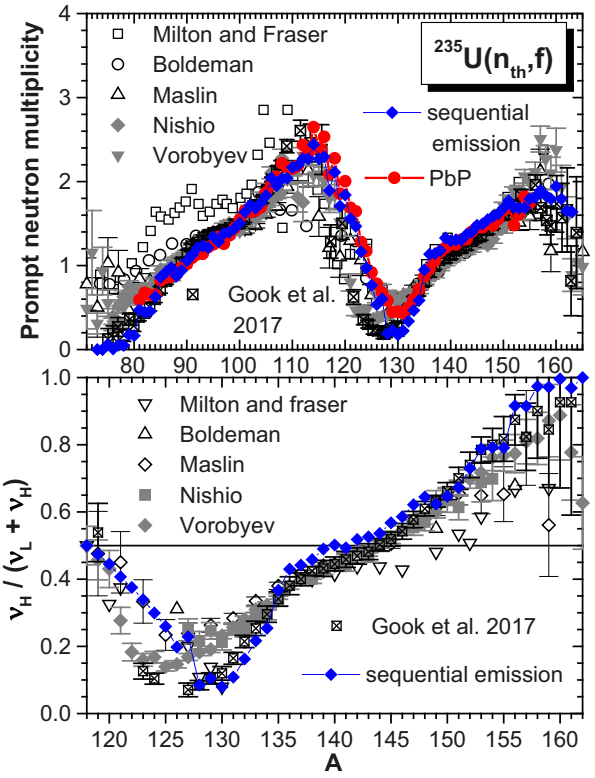

Fig. 9. $\overline{\nu}(A)$ (upper part) and the ratio $\nu_H/(\nu_L+\nu_H)$ as a function of A_H for ^{235}U(n_{th}, f): the sequential emission result (blue diamonds) in comparison with the experimental data (different black and gray symbols) and the PbP result (red circles) of ref. [4].

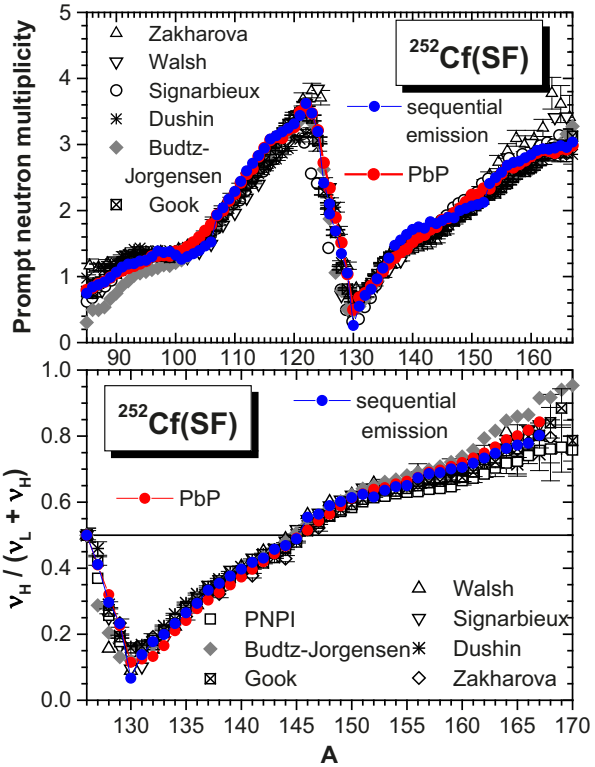

Fig. 10. $\overline{\nu}(A)$ (upper part) and the ratio $\nu_H/(\nu_L+\nu_H)$ as a function of A_H for ^{252}Cf(SF) using the same symbols and colors as in fig. 9.

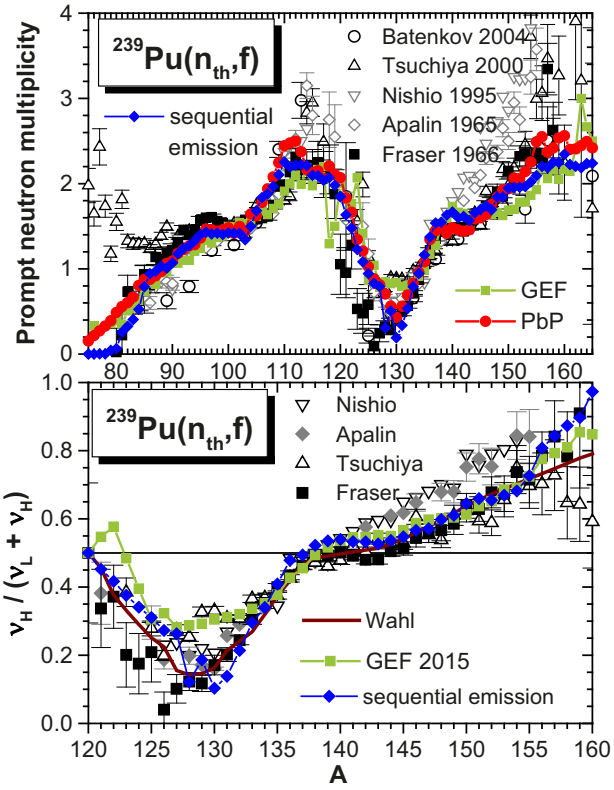

Fig. 11. $\overline{\nu}(A)$ (upper part) and the ratio $\nu_{\rm H}/(\nu_{\rm L}+\nu_{\rm H})$ as a function of $A_{\rm H}$ for ^{239}Pu(n$_{\rm th}$, f): the sequential emission result (blue diamonds), the experimental data (different black and gray symbols), the Wahl evaluation (wine line in the lower part), the results of PbP (red circles) and GEF (green squares).

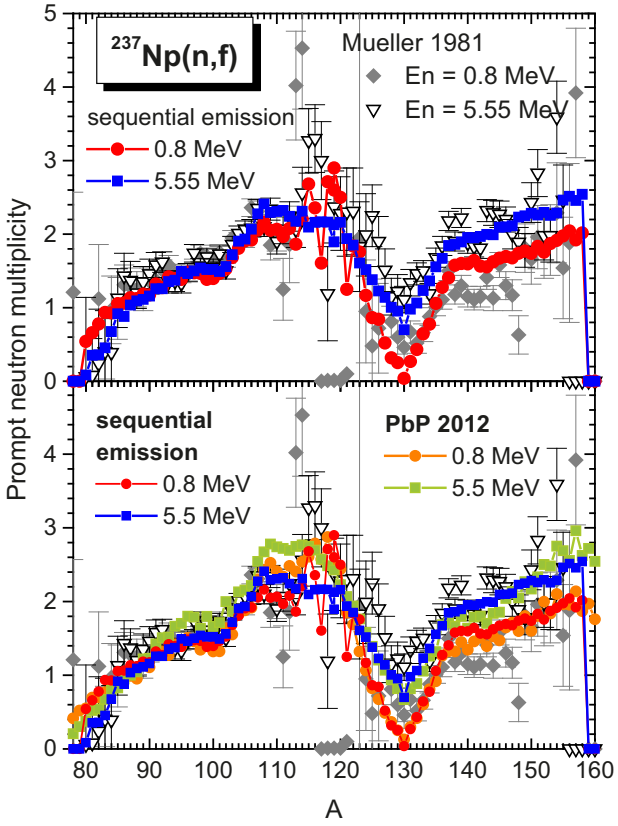

Fig. 12. $\overline{\nu}(A)$ of ^{237}Np(n, f) at $En = 0.8$ and 5.5 MeV: the sequential emission results are plotted with red circles (0.8 MeV) and blue squares (5.5 MeV), the experimental data are plotted with full gray symbols at 0.8 MeV and open black symbols at 5.55 MeV. The PbP results are given in the lower part with orange circles (0.8 MeV) and green squares (5.5 MeV).

$\nu_{\rm H}/(\nu_{\rm L}+\nu_{\rm H})$ as a function of $A_{\rm H}$ (mentioned by Wahl [12] and in many of our previous papers, *e.g.* refs. [23–25]). At low excitation energy this systematic behaviour consists in a ratio less than 0.5 for $A_{\rm H}$ going from symmetric fission up to about 140, with a minimum placed at $A_{\rm H}$ around 130. The ratio is of about 0.5 at $A_{\rm H}$ around 140 (which corresponds to the most probable fragmentation of the majority of fissioning nuclei) and it exhibits an almost linear increase for $A_{\rm H}$ above this value. Such comparisons are illustrated in figs. 9–11 for ^{235}U(n$_{\rm th}$, f), ^{252}Cf(SF) and ^{239}Pu(n$_{\rm th}$, f): $\overline{\nu}(A)$ in the upper part and the ratio $\nu_{\rm H}/(\nu_{\rm L}+\nu_{\rm H})$ as a function of $A_{\rm H}$ in the lower part. The sequential emission results are plotted with blue symbols, the experimental data with different black and gray symbols and the PbP results of ref. [4] with red circles. In the case of ^{239}Pu(n$_{\rm th}$, f) the result of the GEF code [26] is also given (green symbols).

As it can be seen the sequential emission results of $\overline{\nu}(A)$ and the ratio $\nu_{\rm H}/(\nu_{\rm L}+\nu_{\rm H})$ as a function of $A_{\rm H}$, give an overall good description of the experimental data of these fissioning nuclei.

In the case of ^{235}U(n$_{\rm th}$, f) (fig. 9) the sequential emission result of $\overline{\nu}(A)$ at $A_{\rm H}$ around 130 is visibly lower than the PbP result and the experimental data, except the data of Göök *et al.* [27]. A slight overestimation of experimental data at $A_{\rm H}$ between 140 and 145 is also seen, being more visible in the ratio $\nu_{\rm H}/(\nu_{\rm L}+\nu_{\rm H})$ as a function of $A_{\rm H}$.

In the case of ^{252}Cf(SF) (fig. 10) the sequential emission result of both $\overline{\nu}(A)$ and the ratio $\nu_{\rm H}/\nu_{\rm pair}(A_{\rm H})$ gives a very good description of experimental data, including the recent ones of Göök *et al.* [6] (black squares with a cross inside).

The lower value of $\overline{\nu}(A)$ provided by the sequential emission calculation at $A_{\rm H}$ around 130 compared to the PbP results and the majority of experimental data is visible in the case of ^{252}Cf(SF) and ^{239}Pu(n$_{\rm th}$, f), too. This fact is not surprising because the sequential emission calculations were done by taking only three charge numbers Z at each A. Consequently the three nuclei considered at $A_{\rm H}$ around 130, being often magic ($N = 82$) and double magic ($N = 82$, $Z = 50$), in many cases they have not sufficient excitation energy to emit neutrons, leading to a low average $\overline{\nu}(A)$ (obtained by averaging $\nu(A, Z, {\rm TKE})$ given by eq. (12) over $Y(A, Z, {\rm TKE})$ by summing over Z and TKE). This is not happening in the case of the PbP model when the sequential emission is globally treated by

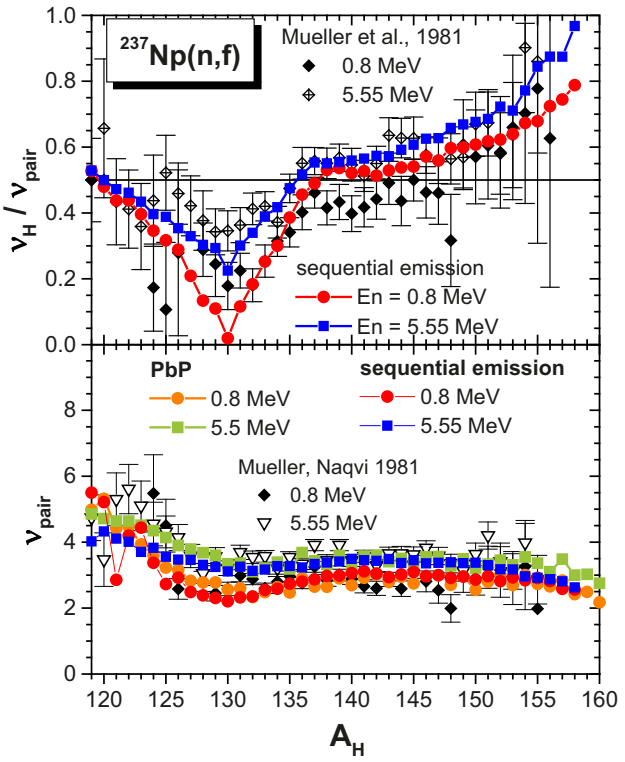

Fig. 13. Upper part: sequential emission results of the ratio $\nu_{\rm H}/\nu_{\rm pair}(A_{\rm H})$ at $En = 0.8$ MeV (red circles) and 5.5 MeV (blue squares) in comparison with the experimental data (full symbols at 0.8 MeV and symbols with a cross inside at 5.55 MeV). Lower part $\overline{\nu}_{\rm pair}(A_{\rm H})$ of sequential emission (same symbols and colors as in the upper part) in comparison with the PbP results (orange circles at 0.8 MeV and green squares at 5.5 MeV) and the experimental data (full black symbols at 0.8 MeV and open symbols at 5.5 MeV).

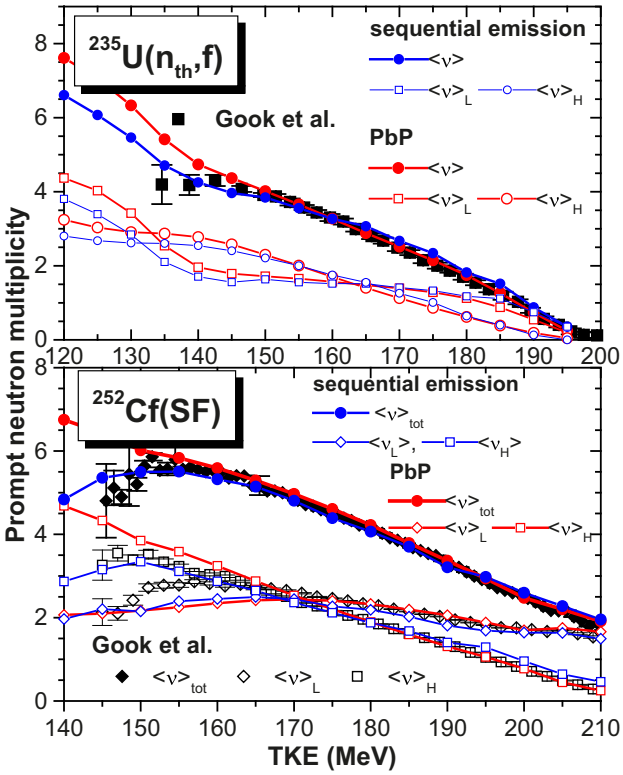

Fig. 14. $\langle\nu\rangle$(TKE) of ^{235}U(n, f) (upper part) and ^{252}Cf(SF) (lower part): the sequential emission results are plotted with blue symbols, the experimental data of Göök *et al.* [6,32] with black symbols and the PbP results with red symbols.

an analytical function of the residual temperature distribution.

The sequential emission results of $\overline{\nu}(A)$ of ^{237}Np(n, f) at $En = 0.8$ MeV and 5.5 MeV are plotted in fig. 12 with red circles and blue squares, respectively, in the upper part only in comparison with the experimental data sets of Mueller *et al.* [28] (full gray symbols at 0.8 MeV and open black symbols at 5.55 MeV) and in the lower part also in comparison with the PbP results of ref. [14] (orange circles at 0.8 MeV and green squares at 5.5 MeV).

Prompt neutron multiplicity increase with incident energy mainly for heavy fragments is clearly visible in both calculations.

The behaviour of the prompt neutron multiplicity ratio $\nu_{\rm H}/(\nu_{\rm L}+\nu_{\rm H})$ as a function of $A_{\rm H}$ with increasing incident neutron energy is well revealed in the upper part of fig. 13 where the sequential emission results are plotted with red circles at $En = 0.8$ MeV and blue squares at $En = 5.5$ MeV in comparison with the experimental data (full black symbols at 0.8 MeV and black symbols with a cross inside at 5.55 MeV). The increase of the minimum placed at $A_{\rm H}$ around 130 with increasing En is clearly visible, as well as a slight increase above 0.5 at $A_{\rm H}$ around 140 (due to the multiplicity increase with En for heavy fragments only). This is a typical behaviour of the $\nu_{\rm H}/(\nu_{\rm L}+\nu_{\rm H})$ ratio with increasing En (for details see refs. [29,30]).

The comparable prompt neutron multiplicity results of sequential emission and PbP is better visible in the lower part of fig. 13 where the prompt neutron multiplicity of a fragment pair is plotted as a function of $A_{\rm H}$ with the same symbols and colors as in the lower part of fig. 12.

The sequential emission results of $\langle\nu\rangle$(TKE) (blue symbols) are also in very good agreement with the recent experimental data of ^{235}U(n, f) and ^{252}Cf(SF) measured by Göök *et al.* [6,27] (black symbols) as it can be seen in fig. 14. The PbP results are also given (red symbols) for comparison.

For both fissioning systems differences between the sequential emission and PbP results are visible only at low TKE values, where $\langle\nu\rangle$(TKE) of sequential emission is lower. This is due also to the limited number of nuclei taken at each A in the sequential treatment, while in the PbP treatment, even if the fragmentation range is the same, this situation is avoided by the global treatment of the sequential emission using a function of the residual temperature distribution.

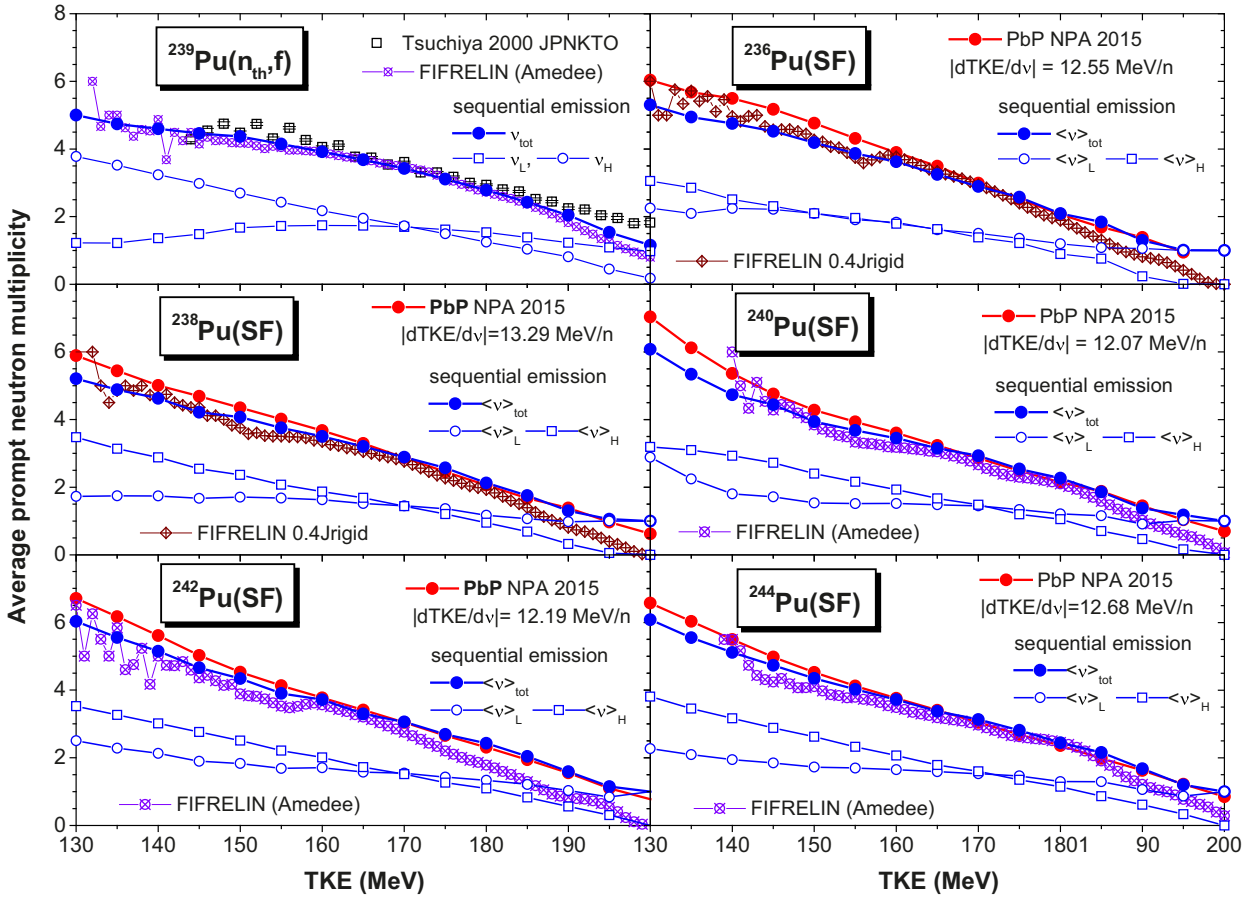

Fig. 15. Sequential emission results of $\langle\nu\rangle$(TKE) (blue symbols) for ^{239}Pu(n$_{\rm th}$, f) and $^{236-244}$Pu(SF): in comparison with experimental data (open black symbols) and the results of prompt emission models PbP (red circles) and FIFRELIN (wine or violet symbols).

Sequential emission results of $\langle\nu\rangle$(TKE) for other studied fissioning systems, *i.e.* ^{239}Pu(n$_{\rm th}$, f) and the spontaneous fission of the even-even Pu isotopes $^{236-244}$Pu, are given in fig. 15. Because experimental $\langle\nu\rangle$(TKE) data exist only for ^{239}Pu(n$_{\rm th}$, f) being missing for $^{236-244}$Pu(SF), the present sequential emission results of $\langle\nu\rangle$(TKE) are compared with the PbP results (red symbols) and the results of the FIFRELIN code (based on sequential emission in the frame of a probabilistic Monte Carlo treatment). These results taken from ref. [31] are plotted with symbols with a cross inside in different colors according to the prescriptions used for the inertial momentum.

As it can be seen in fig. 15, the $\langle\nu\rangle$(TKE) results of sequential emission are close to those of FIFRELIN, including at low TKE values. They are also close to the PbP results at medium and high TKE values and are lower than PbP at low TKE for the same reason already mentioned related to fig. 14.

The average center-of-mass energy of prompt neutrons resulting from sequential emission is plotted with blue symbols in the upper part of fig. 16 in comparison with the recent experimental $\langle\varepsilon\rangle(A)$ data of ^{235}U(n, f) and ^{252}Cf(SF) measured by Göök *et al.* [6,32] (full black squares). The $\langle\varepsilon\rangle(A)$ results of PbP from ref. [4] (red circles) and of the Monte Carlo codes based on sequential emission FIFRELIN (open wine circles), CGMF (green diamonds with a cross inside) and FREYA (open orange triangles) reported in ref. [3] are also given for comparison. The present $\langle\varepsilon\rangle(A)$ results of sequential emission are in agreement with the experimental data, except at $A_{\rm H}$ around 130 where they are much lower than the data and the results of PbP, FIFRELIN and CGMF, being close to the FREYA result in the case of ^{235}U(n$_{\rm th}$, f). This underestimation is due not only to the limited number of three Z taken at each A but especially to the non-energy level density parameters of the Egidy-Bucurescu systematic for the BSFG model. As it was already mentioned in sect. 2.2, they lead to much lower values of $\langle\varepsilon\rangle$ for residual fragments with $A_{\rm H}$ around 130 at low excitation energies (below 5–6 MeV) than those corresponding to the energy-dependent level density parameters of the super-fluid model.

The same situation (*i.e.*, low values at $A_{\rm H}$ around 130) is happening for the energy carried out per neutron $\eta(A)$ (defined as $\eta = \langle\varepsilon\rangle + S_n$) of ^{252}Cf(SF) given in the lower right part of fig. 16.

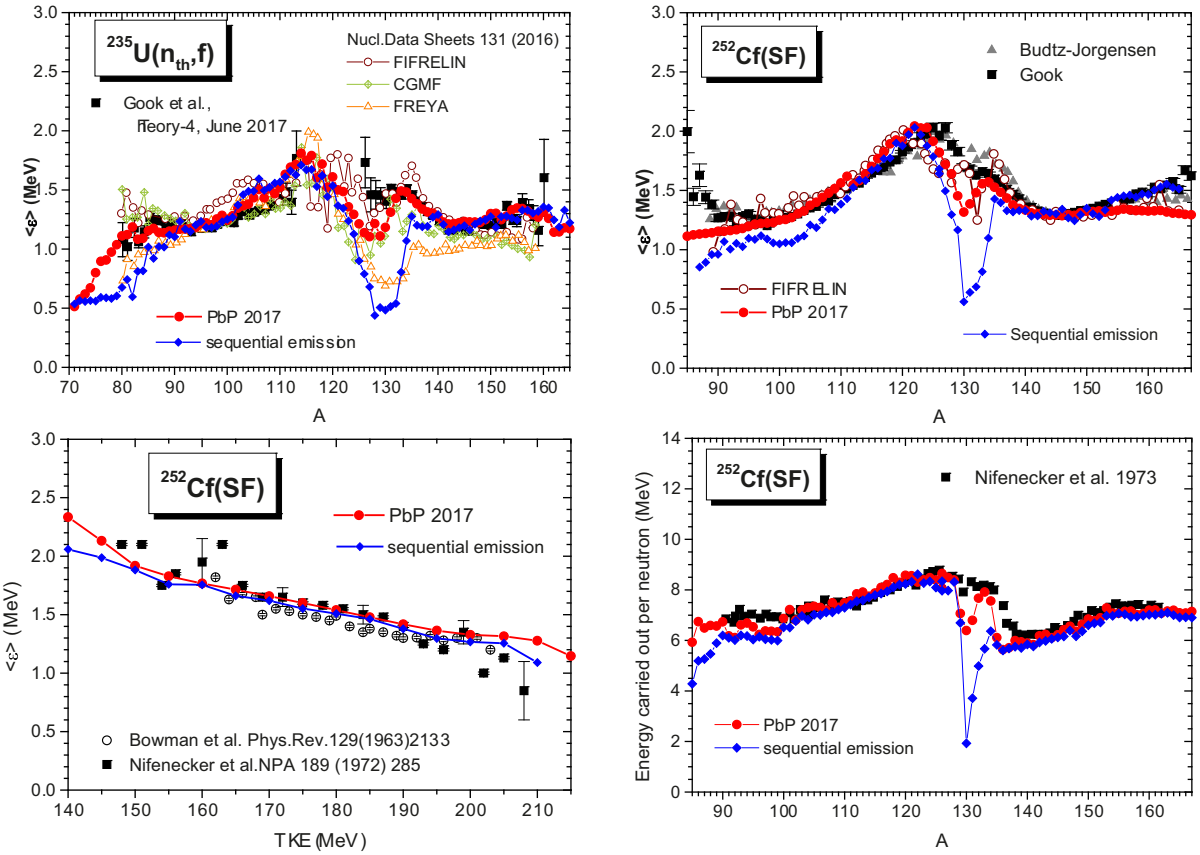

Fig. 16. Upper part $\langle\varepsilon\rangle(A)$ of ^{235}U(n_{th}, f) and ^{252}Cf(SF): the sequential emission result (blue symbols) in comparison with the experimental data (full black and gray symbols) and the results of prompt emission models PbP (red circles), FIFRELIN (open wine symbols), CGMF (green diamonds with a cross) and FREYA (open orange up triangles). Lower part: $\langle\varepsilon\rangle$(TKE) (left) and $\eta(A)$ (right) of ^{252}Cf(SF) the sequential emission result (blue symbols) in comparison with the experimental data (full and open black symbols) and the PbP results (red circles).

The average center-of-mass energy of prompt neutrons as a function of TKE for ^{252}Cf(SF) is plotted in the lower left part of fig. 16. As it can be seen the $\langle\varepsilon\rangle$(TKE) result of sequential emission (blue symbols) agrees with the experimental data (full and open black symbols). It exhibits the same decreasing slope as the PbP result from ref. [4] (red circles).

Sequential emission results of average prompt γ-ray energy $\overline{E}_\gamma(A)$ of ^{235}U(n_{th}, f) and ^{239}Pu(n_{th}, f) describing the experimental data as well as the linear correlation between the average prompt γ-ray energy and average prompt neutron multiplicity were already reported in ref. [33]. Consequently in fig. 17 only the sequential emission result of $\overline{E}_{\gamma\,\mathrm{pair}}(A_\mathrm{H})$ of ^{252}Cf(SF) is given with blue symbols. It is in good agreement with the experimental data of Nifenecker *et al.* [34] (full black squares) and the PbP result of ref. [4] (red circles). At A_H near symmetry the sequential emission result is in better agreement with the experimental data than the PbP result.

Sequential emission results of the prompt neutron multiplicity distribution $P(\nu)$ are plotted with open blue circles in fig. 18 in comparison with the experimental data (different black and gray symbols) and the results of PbP from refs. [4,35,36] (full red circles). The $P(\nu)$ results of sequential emission are in overall good agreement with the experimental data and the PbP model results.

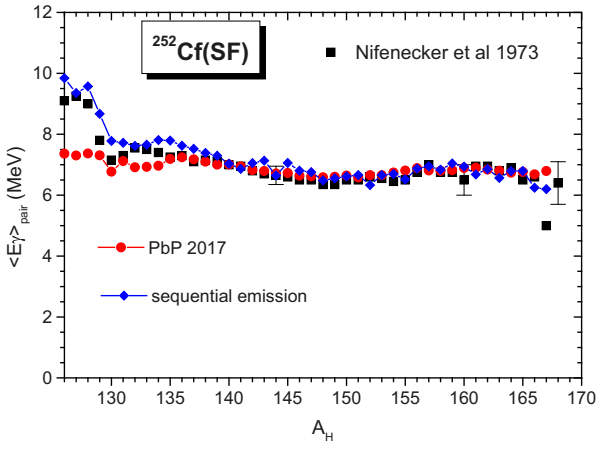

Fig. 17. Average prompt γ-ray energy of a fragment pair as a function of A_H for ^{252}Cf(SF): experimental data of Nifenecker (black squares) and the results of sequential emission (blue diamonds) and PbP (red circles).

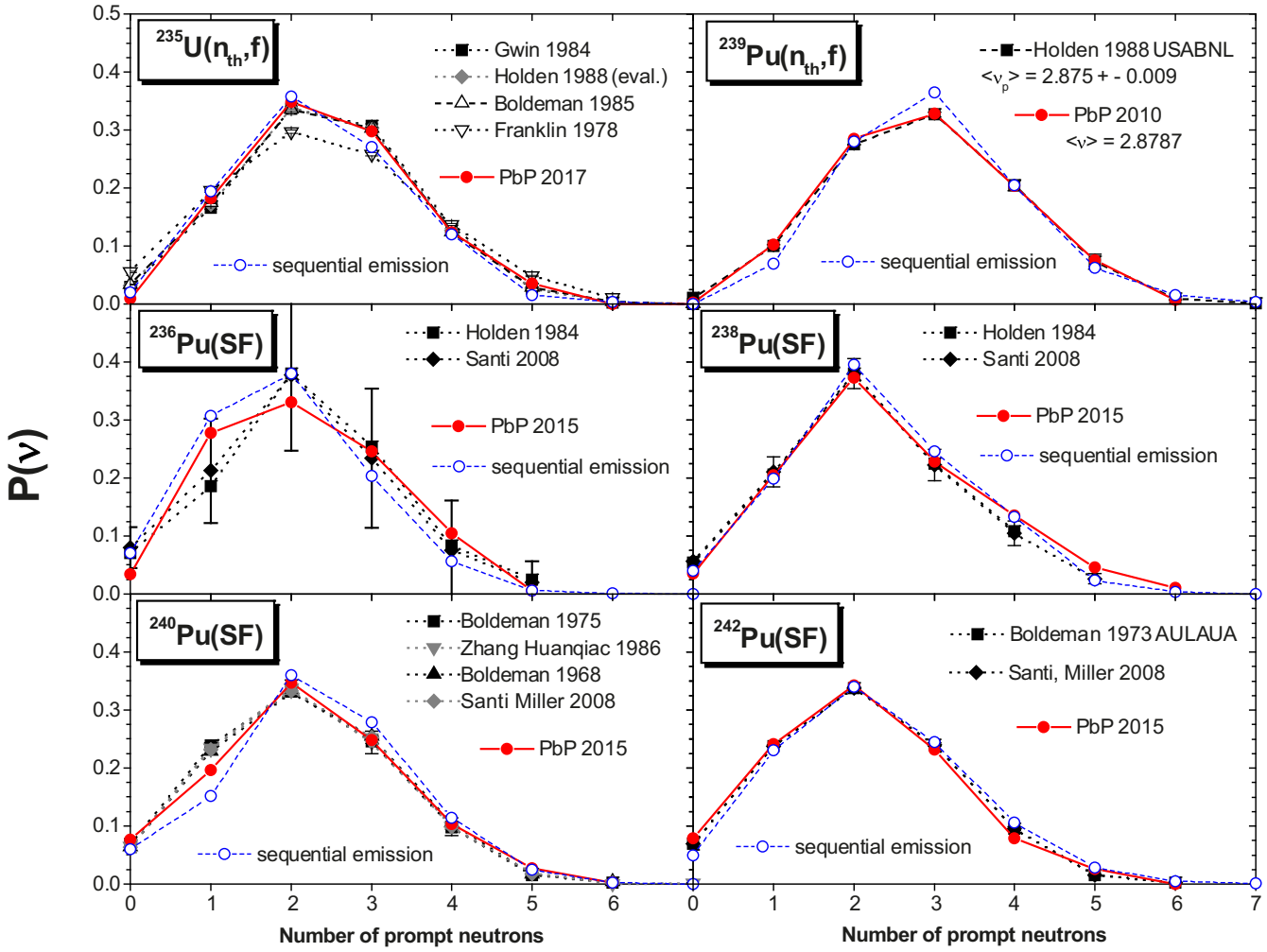

Fig. 18. Sequential emission results of $P(\nu)$ of ^{235}U(n_{th}, f), ^{239}Pu(n_{th}, f) and $^{236-242}$Pu(SF) (open blue circles connected with dashed lines) in comparison with experimental data (different black and gray symbols connected with dashed or dotted lines) and the results of PbP (full red circles connected with solid lines) from refs. [4,35,36].

Prompt fission neutron spectra in the laboratory frame were also calculated as following. The Weisskopf-Ewing evaporation spectra of each emitted neutron, indexed k, corresponding to an initial fragment A, Z, TKE, *i.e.* $\varphi_k(\varepsilon) = K(T_k)\sigma_c^{(k-1)}(\varepsilon)\varepsilon\exp(-\varepsilon/T_k)$ with $\sigma_c(\varepsilon)$ of eq. (6), are averaged over the number of sequences $k_{\max}(A, Z, \mathrm{TKE})$ according to eq. (12), giving the average prompt neutron spectrum in the center-of-mass frame $\overline{\varphi}(\varepsilon, A, Z, \mathrm{TKE})$ corresponding to an initial fragment $\{A, Z\}$ at a given TKE. This spectrum is transformed into the laboratory frame,

$$N(E, A, Z, \mathrm{TKE}) = \frac{1}{4\sqrt{E_f(A, Z, \mathrm{TKE})}} \times \int_{u1}^{u2} \overline{\varphi}(\varepsilon, A, Z, \mathrm{TKE})\frac{\mathrm{d}\varepsilon}{\sqrt{\varepsilon}} \quad (13)$$

with the integration limits

$$u_{1,2} = \left(\sqrt{\varepsilon} \mp \sqrt{E_f(A, Z, \mathrm{TKE})}\right)^2 \quad (14)$$

and the average kinetic energy per nucleon

$$E_f(A, Z, \mathrm{TKE}) = \frac{A_0 - A}{A}\frac{\mathrm{TKE}}{A_0}, \quad (15)$$

in which A_0 is the mass number of the fissioning nucleus.

The prompt neutron spectrum in the laboratory frame corresponding to a pair of initial fragments (*i.e.*, a fragmentation) at a given TKE value is calculated as

$$N_{\mathrm{pair}}(E) = \frac{\nu_{\mathrm{L}}}{\nu_{\mathrm{L}} + \nu_{\mathrm{H}}}N_{\mathrm{L}}(E) + \frac{\nu_{\mathrm{H}}}{\nu_{\mathrm{L}} + \nu_{\mathrm{H}}}N_{\mathrm{H}}(E), \quad (16)$$

where $N_{\mathrm{L}}(E)$ and $N_{\mathrm{H}}(E)$ are given by eq. (13) and the prompt neutron multiplicities ν_{L} and ν_{H} are those corresponding to complementary initial fragments given by eq. (12).

The total prompt neutron spectrum in the laboratory frame, which can be compared with experimental data, is obtained by averaging the spectra of eq. (16) over the fragment distribution $Y(A, Z, \mathrm{TKE})$. Examples of such prompt neutron spectra in comparison with the

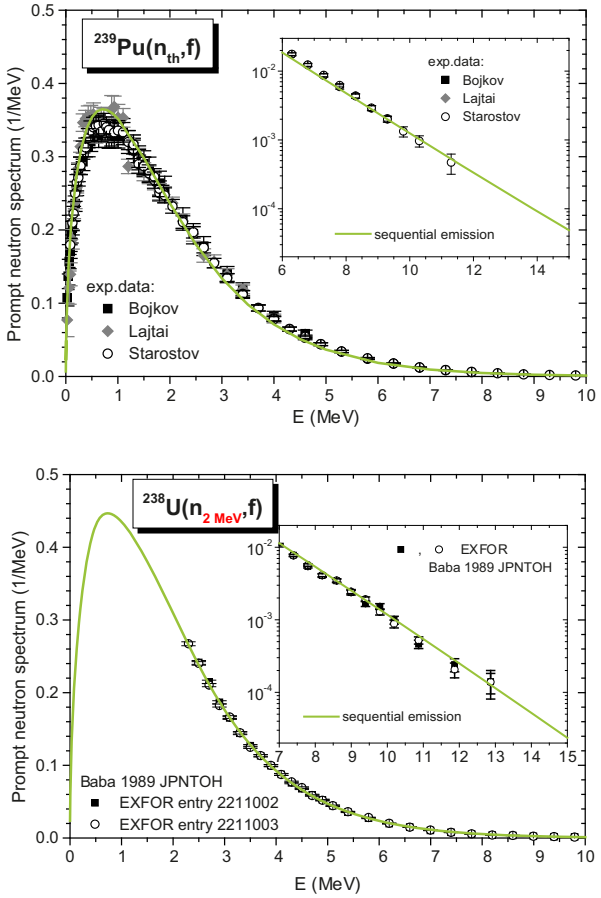

Fig. 19. Prompt fission neutron spectrum of $^{239}\mathrm{Pu}(\mathrm{n_{th}},\mathrm{f})$ (upper part) and $^{238}\mathrm{U}(\mathrm{n_{2\,MeV}},\mathrm{f})$ (lower part) resulting from sequential emission calculation (green line) in comparison with the experimental data renormalized to the respective calculation (different black and gray symbols). The high energy part of the spectrum is focused as an insert.

experimental data (renormalized to the respective calculation) are given in fig. 19 for $^{239}\mathrm{Pu}(\mathrm{n_{th}},\mathrm{f})$ (upper part) and $^{238}\mathrm{U}(\mathrm{n},\mathrm{f})$ at $En = 2\,\mathrm{MeV}$ (lower part). To see better the spectra at high prompt neutron energies, they are given separately as an insert. In both cases the sequential emission result gives an overall good description of experimental spectrum data.

5 Triangular form of the residual temperature distribution

All residual temperature distributions, *i.e.* those corresponding to the emission of the first few neutrons (see fig. 3) as well as the sum of residual temperature distributions following the emission of all successive neutrons from light fragments, heavy fragments and all fragments (given in the figures of this section), can be approximated by a triangular shape with a moderately broad cutoff at high temperatures. See as an example the triangular shapes plotted with blue and green lines in fig. 20. These shapes

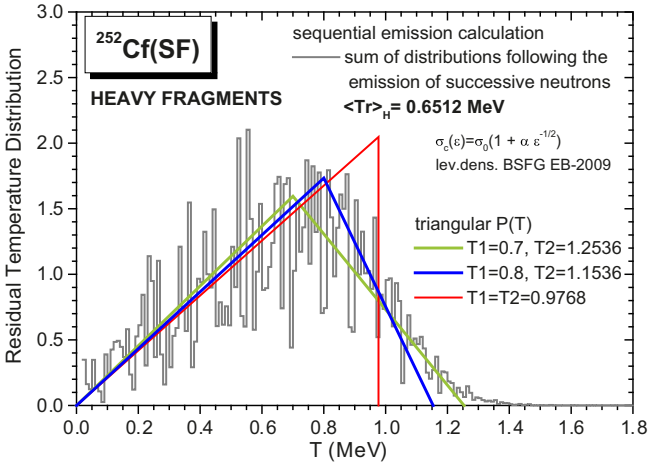

Fig. 20. Illustration of a residual temperature distribution resulting from sequential emission (gray line) approximated by triangular distributions with a broad high temperature cutoff (blue and green lines) and with a sharp cut-off (red line).

approximate the residual temperature distribution resulting from sequential emission calculation, which is plotted as a histogram with a gray line.

The triangular residual temperature distribution is given by the general expression:

$$P(T) = \begin{cases} \dfrac{P_{\max}}{T_1} T, & T \le T_1, \\ \dfrac{P_{\max}}{T_2 - T_1}(T_2 - T), & T_1 \le T \le T_2. \end{cases} \tag{17}$$

The parameters T_1, T_2 and $P_{\max}$ entering this expression can be interrelated by taking into account the following conditions which have to be accomplished by the triangular form of $P(T)$:

i) The normalization to unity, *i.e.* $\int_0^{T_2} P(T)\mathrm{d}T = 1$, from which

$$P_{\max} = 2/T_2 \tag{18}$$

and

ii) the first order momentum of the triangular $P(T)$ of eq. (17) must be equal to the average residual temperature $\langle T_r \rangle$ obtained from sequential emission calculations, *i.e.* $\int_0^{T_2} TP(T)\mathrm{d}T = \langle T_r \rangle$ which leads to the relation

$$T_1 + T_2 = 3\langle T_r \rangle. \tag{19}$$

Taking into account the relations (18) and (19), $P(T)$ of eq. (17) becomes

$$P(T) = \begin{cases} \dfrac{2T}{T_1(3\langle T_r \rangle - T_1)}, & T \le T_1, \\ \dfrac{2}{3\langle T_r \rangle - T_1} \dfrac{3\langle T_r \rangle - T_1 - T}{3\langle T_r \rangle - 2T_1}, & T_1 \le T \le 3\langle T_r \rangle - T_1. \end{cases} \tag{20}$$

Table 1. The ratio of the average residual temperature to the average initial temperature $\langle T_r\rangle/\langle T_i\rangle$.

Fissioning nucleus	$\langle T_r\rangle/\langle T_i\rangle$ light fragments	$\langle T_r\rangle/\langle T_i\rangle$ heavy fragments	$\langle T_r\rangle/\langle T_i\rangle$ all fragments	Prescriptions of the level density parameters and $\sigma_c(\varepsilon)$
^{235}U(n_{th}, f)	0.598	0.589	0.588	BSFG, $\sigma_c(\varepsilon)$ of eq. (6)
	0.594	0.583	0.583	BSFG, σ_c constant
	0.604	0.591	0.595	G-C, $\sigma_c(\varepsilon)$ of eq. (6)
^{252}Cf(SF)	0.623	0.598	0.603	BSFG, $\sigma_c(\varepsilon)$ of eq. (6)
	0.622	0.590	0.599	BSFG, σ_c constant
	0.629	0.600	0.607	G-C, $\sigma_c(\varepsilon)$ of eq. (6)
^{239}Pu(n_{th}, f)	0.614	0.605	0.604	BSFG, $\sigma_c(\varepsilon)$ of eq. (6)
	0.623	0.611	0.615	G-C, $\sigma_c(\varepsilon)$ of eq. (6)
^{236}Pu(SF)	0.599	0.593	0.594	BSFG, $\sigma_c(\varepsilon)$ of eq. (6)
^{238}Pu(SF)	0.595	0.597	0.591	BSFG, $\sigma_c(\varepsilon)$ of eq. (6)
^{240}Pu(SF)	0.591	0.592	0.596	BSFG, $\sigma_c(\varepsilon)$ of eq. (6)
^{242}Pu(SF)	0.602	0.593	0.593	BSFG, $\sigma_c(\varepsilon)$ of eq. (6)
^{244}Pu(SF)	0.604	0.598	0.595	BSFG, $\sigma_c(\varepsilon)$ of eq. (6)

Examples of triangular $P(T)$ forms corresponding to an average residual temperature value $\langle T_r\rangle = 0.6512$ MeV (resulting from the sequential emission calculation for the heavy fragments of ^{252}Cf(SF)) are exemplified in fig. 20 for the T_1 values of 0.7 MeV (green line) and 0.8 MeV (blue line).

The diffuse high temperature cutoff of $P(T)$ can be replaced by a sharp cutoff so that $P(T)$ is given by the following triangular distribution:

$$P(T) = \begin{cases} \dfrac{8T}{9\langle T_r\rangle^2}, & T \leq \dfrac{3}{2}\langle T_r\rangle, \\ 0, & T > \dfrac{3}{2}\langle T_r\rangle, \end{cases} \tag{21}$$

which is plotted with a red line in fig. 20.

The replacement of a triangular $P(T)$ distribution with a moderately broad cutoff at high temperatures by a distribution with a sharp cutoff is justified by the use of this residual temperature distribution with a Weisskopf evaporation spectrum. It is known that the Weisskopf-Ewing spectrum overestimates somewhat the prompt neutron spectra at high neutron energies [1,22]. This overestimation can be compensated by the triangular $P(T)$ with a sharp cutoff which eliminates the residual temperatures higher than the maximum temperature $T_1 = 3\langle T_r\rangle/2$.

The prompt emission models with a global treatment of the sequential emission (*e.g.*, the Los Alamos model of Madland and Nix with equal maximum temperatures of the complementary light and heavy fragments [1] or non-equal maximum temperatures of Madland and Kahler [2] and the PbP model ref. [4] and references therein) consider a residual temperature distribution $P(T)$, *i.e.* the prompt neutron spectrum in the center-of-mass frame expressed as

$$\phi(\varepsilon) = \int_0^{T\,\max} P(T)\varphi(\varepsilon, T)\mathrm{d}T, \tag{22}$$

in which the prompt neutron spectrum corresponding to a given residual temperature T is usually taken as a Weisskopf evaporation spectrum (eq. (2)).

Consequently a triangular $P(T)$ form with a sharp high temperature cutoff, expressed by eq. (21), is used. In this case a connection between the average residual temperature $\langle T_r\rangle$ entering eq. (21) and the temperature of initial fragments T_i (before emission of prompt neutrons) is required. In other words $\langle T_r\rangle$ must be expressed as a function of T_i.

A very interesting finding of this study is that the ratio of average residual temperature $\langle T_r\rangle$ resulting from sequential emission calculations to the initial temperature $\langle T_i\rangle$ is approximately 0.6 in all cases, *i.e.* corresponding to the light and heavy fragment groups and all fragments and for all studied fissioning systems, see table 1 and fig. 21. Even by solving the successive residual temperature equations under different prescriptions of the level density parameter and $\sigma_c(\varepsilon)$, the ratio $\langle T_r\rangle/\langle T_i\rangle$ does not change, it remains ≈ 0.6 (as is exemplified in table 1 for the fissioning nuclei ^{235}U(n_{th}, f), ^{252}Cf(SF) and ^{239}Pu(n_{th}, f)).

It is also very interesting to observe that the ratio $\langle T_r\rangle/\langle T_i\rangle$ does not change with increasing excitation energy of the fissioning nucleus (*i.e.* increasing incident neutron energy En). It remains very close to 0.6. This is shown in the right part of fig. 21 for the fissioning nuclei ^{237}Np(n, f), ^{238}U(n, f) and ^{234}U(n, f) for which sequential emission calculations were done at En values up to about the threshold of second chance fission. In the left part of this figure the average residual and initial temperatures (full and open symbols, respectively) corresponding to the light fragments (blue squares), heavy fragments (red circles) and all fragments (black diamonds) are plotted as a function of En. It can be observed that at low En the average residual temperatures of light fragments are higher than those of heavy fragments. At higher En the situa-

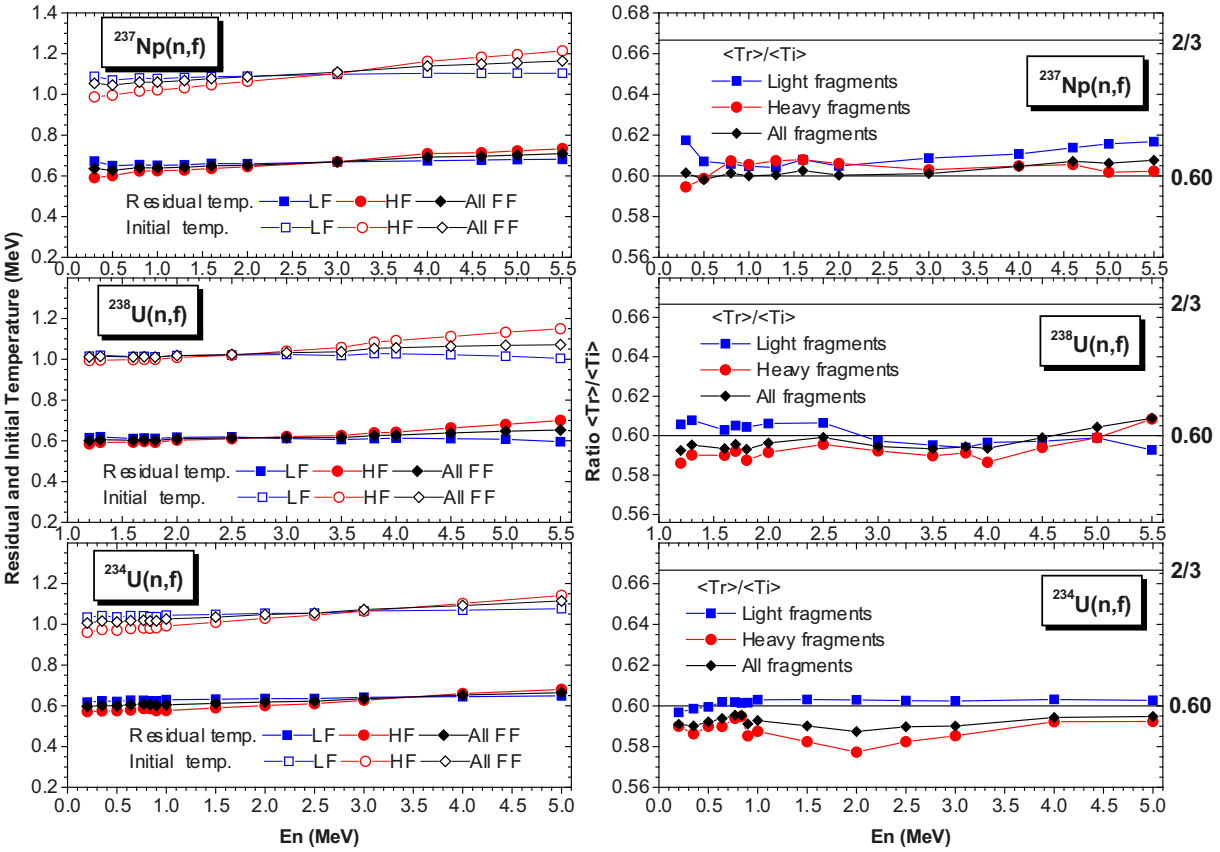

Fig. 21. Left part: the average values of residual temperatures (full symbols) and of initial temperatures (open symbols) corresponding to the light fragments (blue squares), heavy fragments (red circles) and all fragments (black diamonds) as a function of En for ^{237}Np(n, f) (upper part), ^{238}U(n, f) (middle) and ^{234}U(n, f) (lower part). The sequential emission calculations are done at the En values where $Y(A, \mathrm{TKE})$ were measured at JRC-Geel. Right part: the ratios of the average residual temperatures to the average temperatures of the initial fragments at these En values using the same symbols and colors as in the left part. The ratio $\langle \mathrm{Tr} \rangle / \langle \mathrm{Ti} \rangle = 2/3$ corresponding to the $P(T)$ form of Madland and Nix is also plotted.

tion is reversed, $\langle T_r \rangle$ of heavy fragments being higher than $\langle T_r \rangle$ of light fragments. This fact is due to the increase of initial excitation energy and prompt neutron multiplicity with En mainly for the heavy fragments. In the right part of fig. 21 the ratios $\langle T_r \rangle / \langle T_i \rangle$ as a function of En are plotted with the same symbols and colors as in the left part. As it can be seen all $\langle T_r \rangle / \langle T_i \rangle$ ratios are very close to 0.6 over the entire En range.

Consequently by taking $\langle T_r \rangle = 0.6 \langle T_i \rangle$ the triangular $P(T)$ of eq. (20) with a moderately broad cutoff at high temperatures can be expressed as a function of the temperature of the initial fragments (before emission of prompt neutrons) as

$$P(T) = \begin{cases} \dfrac{2}{T_i^2} \dfrac{T}{r(1.8-r)}, & T \le rT_i, \\ \dfrac{2}{T_i^2} \dfrac{1}{1.8-2r} \left(T_i - \dfrac{T}{1.8-r} \right), & rT_i \le T \le (1.8-r)T_i, \end{cases} \tag{23}$$

in which r is a parameter with the maximum value of 0.9.

By considering $\langle T_r \rangle = 0.6 \langle T_i \rangle$ in the triangular $P(T)$ with a sharp cut-off given by eq. (21) or by taking $r = 0.9$ in eq. (23), the following triangular distribution with a sharp high temperature cutoff is obtained

$$P(T) = \begin{cases} \dfrac{2}{T_i^2} \dfrac{T}{0.81}, & T \le 0.9T_i, \\ 0, & T > 0.9T_i. \end{cases} \tag{24}$$

This triangular form of $P(T)$ is similar to the $P(T)$ form proposed by Madland and Nix [1] which is currently used in the Los Alamos and PbP models

$$P(T) = \begin{cases} \dfrac{2}{T_i^2} T, & T \le T_i, \\ 0, & T > T_i, \end{cases} \tag{25}$$

for which the ratio $\langle T_r \rangle / \langle T_i \rangle$ is 2/3. Obviously, by replacing $\langle T_r \rangle = (2/3) \langle T_i \rangle$ in the $P(T)$ form of eq. (21) the $P(T)$ of Madland and Nix is obtained.

The sums of the residual temperature distributions following the successive emission of each neutron from light fragments, heavy fragments and all fragments obtained

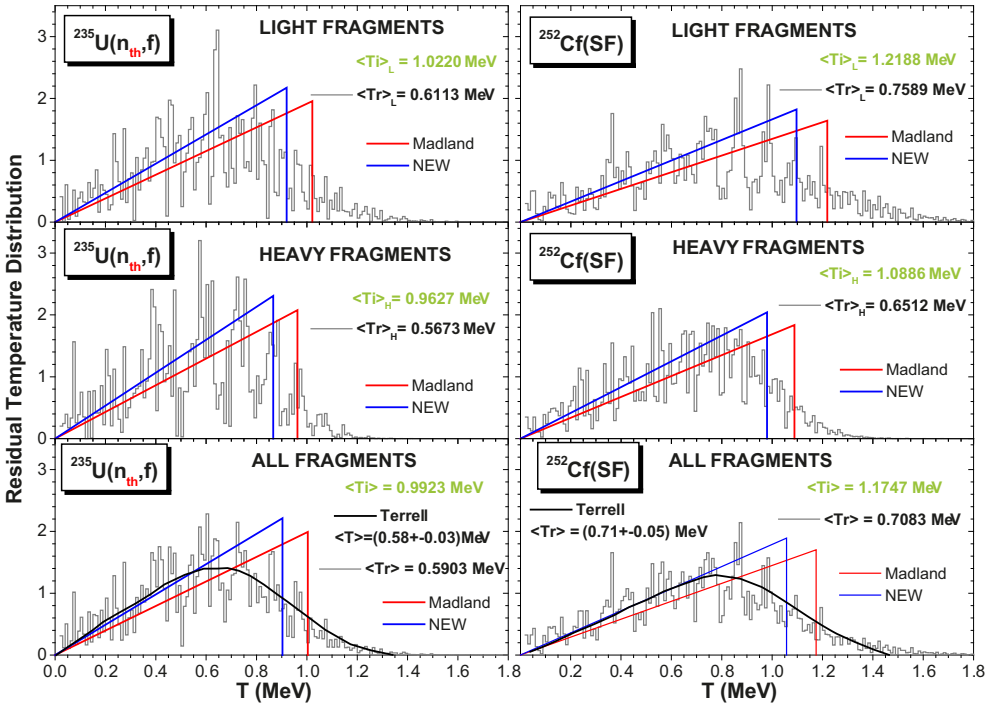

Fig. 22. Residual temperature distributions of ^{235}U(n$_{\rm th}$, f) (left part) and ^{252}Cf(SF) (right part) for light fragments (upper part), heavy fragments (middle) and all fragments (lower part). The $P(T)$ result of sequential emission is given with a gray line. $P(T)$ of Terrell is plotted with a black line in the lower part. The present value of $\langle T_r \rangle$ is in good agreement with the result of Terrell. The $P(T)$ form of Madland and Nix is plotted with a red line and the new $P(T)$ with a blue line. The values of average residual and initial temperatures are indicated in each frame.

from the sequential emission calculations for the fissioning nuclei ^{235}U(n$_{\rm th}$, f), ^{252}Cf(SF) are plotted as histograms (gray lines) in fig. 22. The new $P(T)$ expressed by eq. (24) are given with blue lines in comparison with the $P(T)$ form of Madland and Nix (red lines). The values of average residual and initial temperatures are indicated in each frame.

Residual temperature distributions of these fissioning nuclei, deduced from experimental data available at that time, were reported by Terrell [22]. They are plotted with black lines in the lower parts of fig. 22. As it can be seen the residual temperature distributions from the present sequential emission treatment (gray lines) are in very good agreement with the distributions of Terrell. The average values of the residual temperature corresponding to the sum of residual temperature distributions following the successive emission of each neutron from all fragments are also in very good agreement with the average values reported by Terrell, *i.e.* for ^{235}U(n$_{\rm th}$, f) the present result $\langle T_r \rangle = 0.590\,$MeV compared to $\langle T \rangle = (0.58 \pm 0.30)\,$MeV [22] and for ^{252}Cf(SF) the present result $\langle T_r \rangle = 0.708\,$MeV compared to the result of Terrel $\langle T \rangle = (0.71 \pm 0.05)\,$MeV.

Note, the average residual temperature $\langle T \rangle$ was obtained by Terrell [22] from a relation connecting the average prompt neutron energies in the center-of-mass and laboratory frames and the average kinetic energy per nucleon $\langle E_f \rangle$, *i.e.* $\langle E \rangle = \langle E_f \rangle + \langle \varepsilon \rangle$. Assuming a Weiskopf evaporation spectrum in the center-of-mass frame with a nearly constant $\sigma_c(\varepsilon)$, Terrell has obtained $\langle T \rangle$ from the relation $\langle E \rangle = \langle E_f \rangle + 2\langle T \rangle$ in which $\langle E \rangle$ was determined from experimental prompt neutron spectrum data (*e.g.*, $\langle E \rangle = (1.935 \pm 0.05\,$MeV) in the case of ^{235}U(n$_{\rm th}$, f)). $\langle E_f \rangle$ was obtained from the experimental TKE data available at that time and the fragment mass ratios $A_{\rm H}/A_{\rm L}$. It is interesting to mention the average value $\langle E_f \rangle = (0.78 \pm 0.02)\,$MeV found by Terrell for a wide range of Z and A.

For the fissioning nuclei ^{239}Pu(n$_{\rm th}$, f) and ^{236,238,240,242,244}Pu(SF) the sum of residual temperature distributions following the successive emission of all neutrons a) from light fragments, b) from heavy fragments and c) from all fragments are plotted in fig. 23 together with the new $P(T)$ form of eq. (24) and the $P(T)$ of Madland and Nix, using the same colors as in fig. 22. In the case of ^{237}Np(n, f), ^{238}U(n, f) and ^{234}U(n, f) sequential emission calculations were performed at the incident neutron energies where $Y(A, {\rm TKE})$ distributions were measured. For each of these fissioning nuclei residual temperature distributions are exemplified at two incident energies as following. ^{237}Np(n, f) at $En = 0.8$ and $5.55\,$MeV (fig. 24), ^{238}U(n, f) at $En = 2$ and $5.5\,$MeV (fig. 25) and ^{234}U(n, f) at $En = 0.835$ and $5\,$MeV (fig. 26). The $P(T)$ resulting from sequential emission calculations and the triangular $P(T)$ of eqs. (24) and (25) are plotted with the same colors as in figs. 22 and 23.

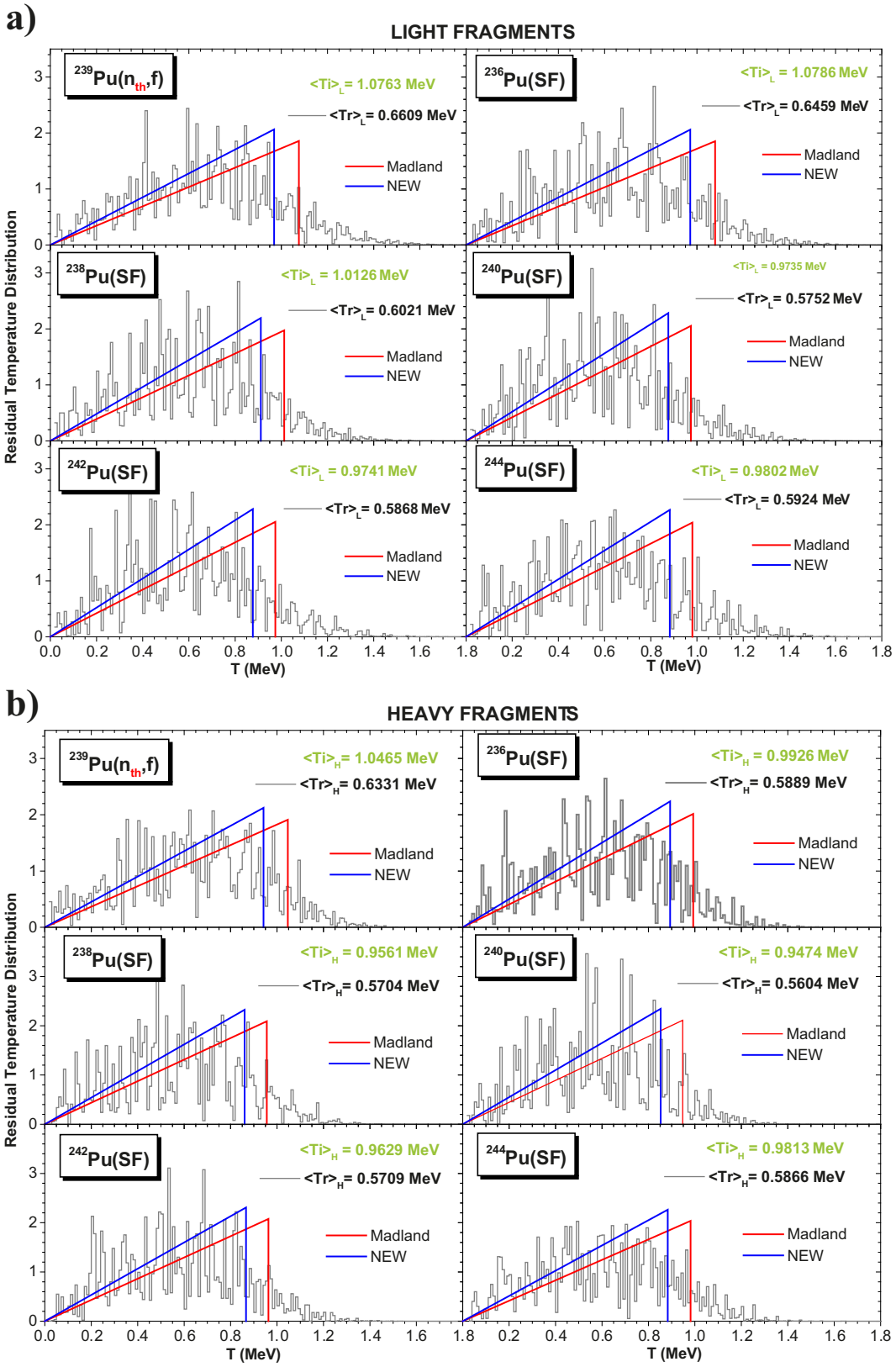

Fig. 23. Residual temperature distributions of ^{239}Pu(n_{th}, f) and $^{236-244}$Pu(SF) of (a) heavy fragments, (b) light fragments and (c) all fragments: $P(T)$ from sequential emission (histogram, gray lines), new $P(T)$ (blue lines) and $P(T)$ of Madland and Nix (red lines). The values of average residual and initial temperatures are indicated in each frame.

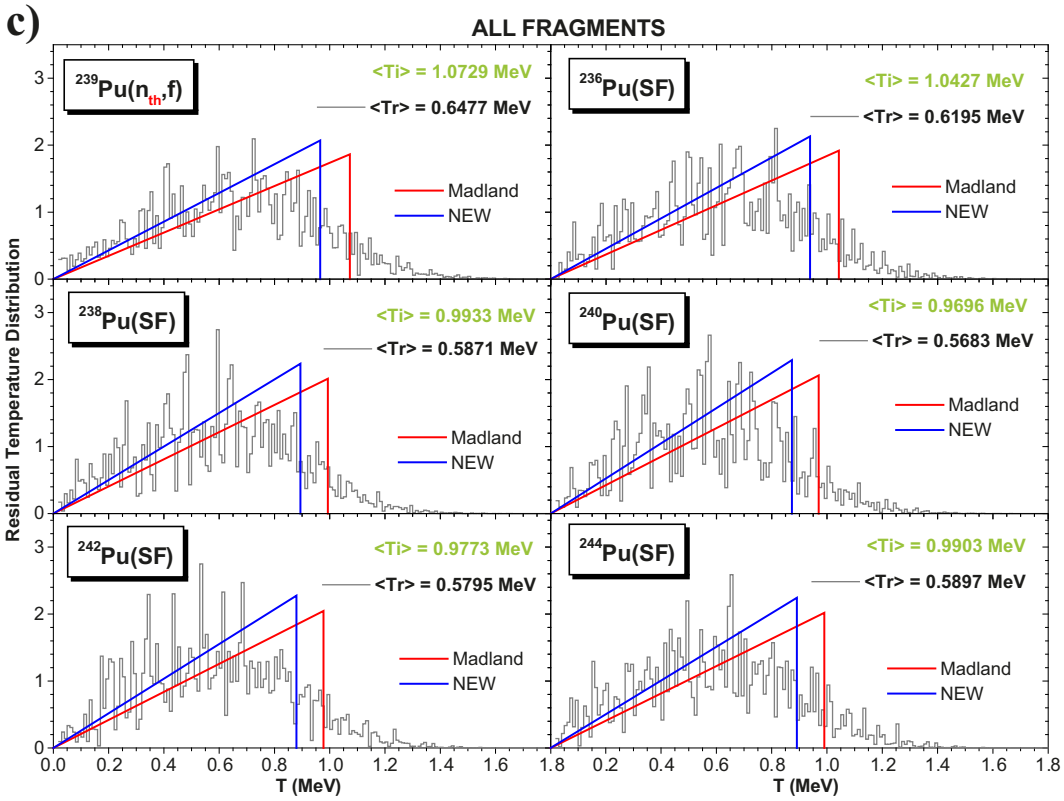

Fig. 23. Continued.

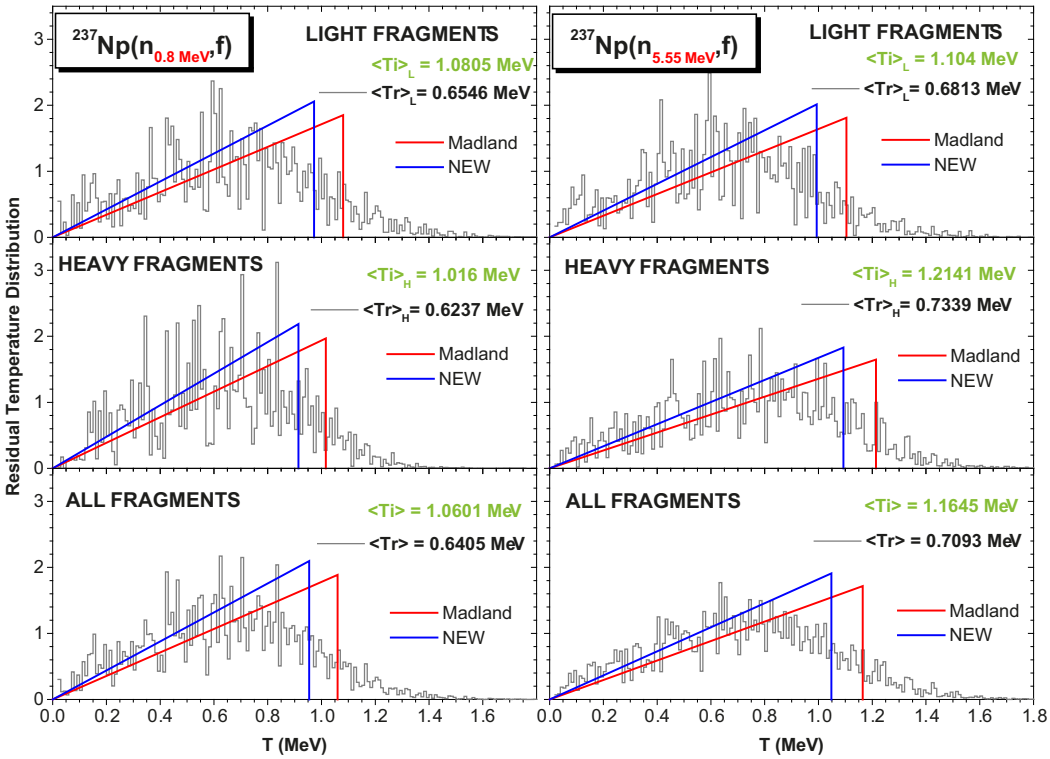

Fig. 24. Residual temperature distributions of ^{237}Np(n, f) at En = 0.8 MeV (left side) and 5.5 MeV (right side) of light fragments (upper part), heavy fragments (middle) and all fragments (lower part) plotted with the same colors as in previous figures.

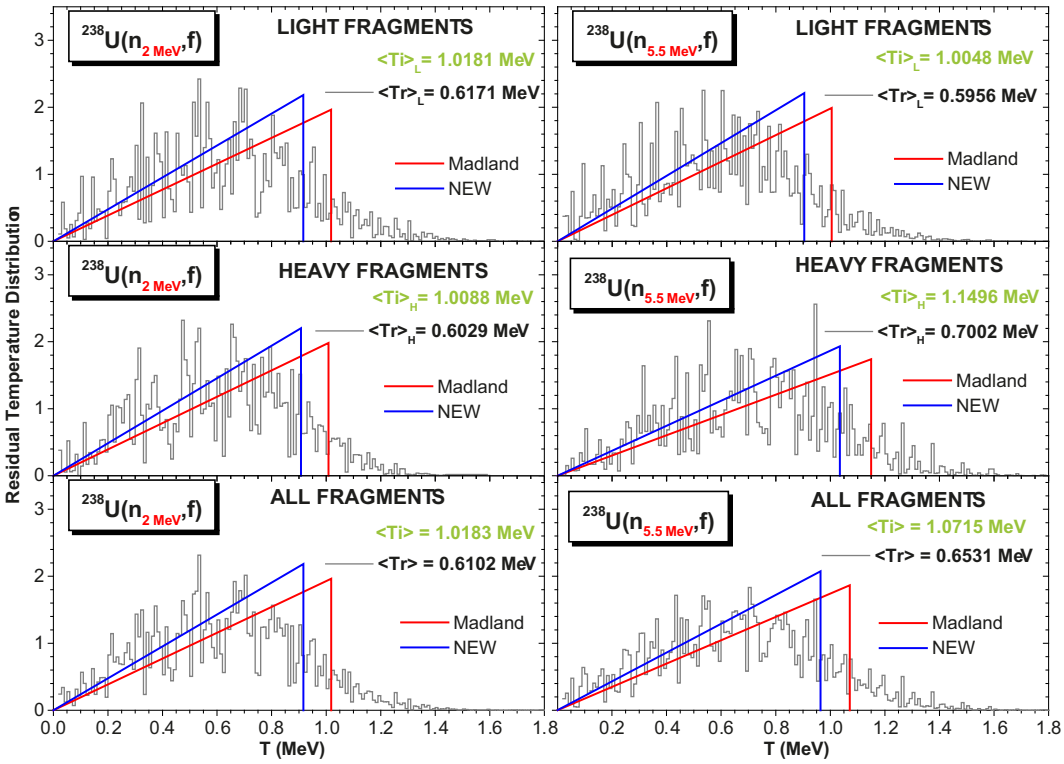

Fig. 25. Residual temperature distributions of ^{238}U(n, f) at $En = 2$ MeV (left side) and 5.5 MeV (right side) of light fragments (upper part), heavy fragments (middle) and all fragments (lower part) plotted with the same colors as in previous figures.

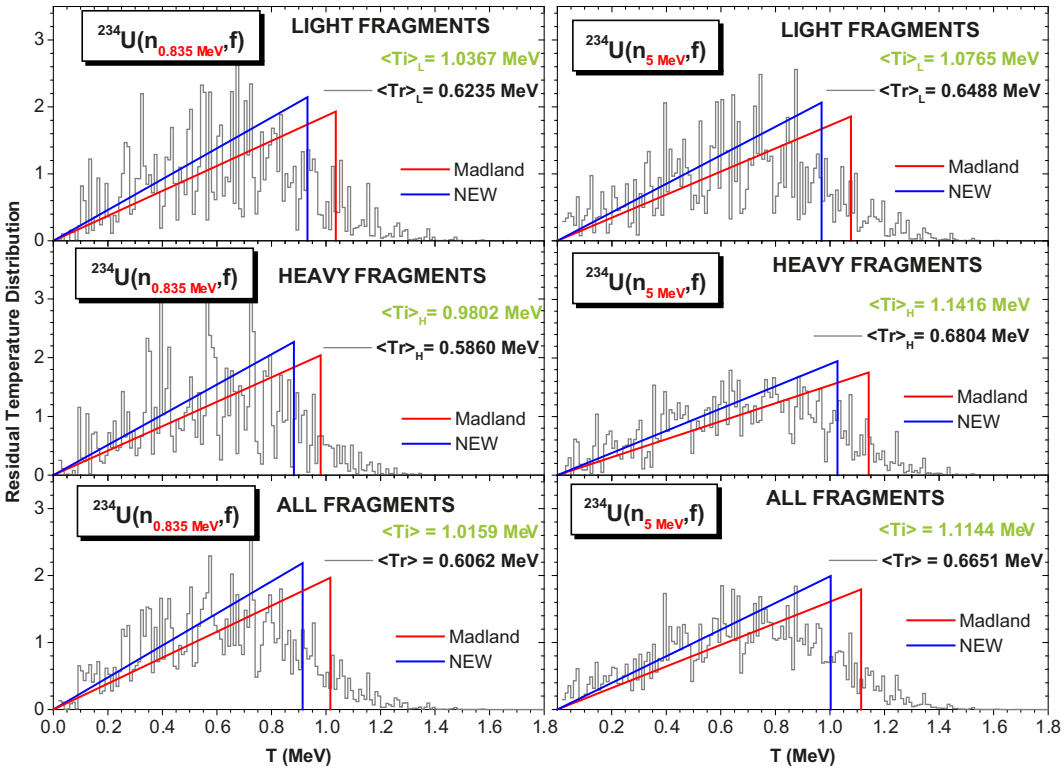

Fig. 26. Residual temperature distributions of ^{234}U(n, f) at $En = 0.835$ MeV (left side) and 5 MeV (right side) of light fragments (upper part), heavy fragments (middle) and all fragments (lower part) plotted with the same colors as in previous figures.

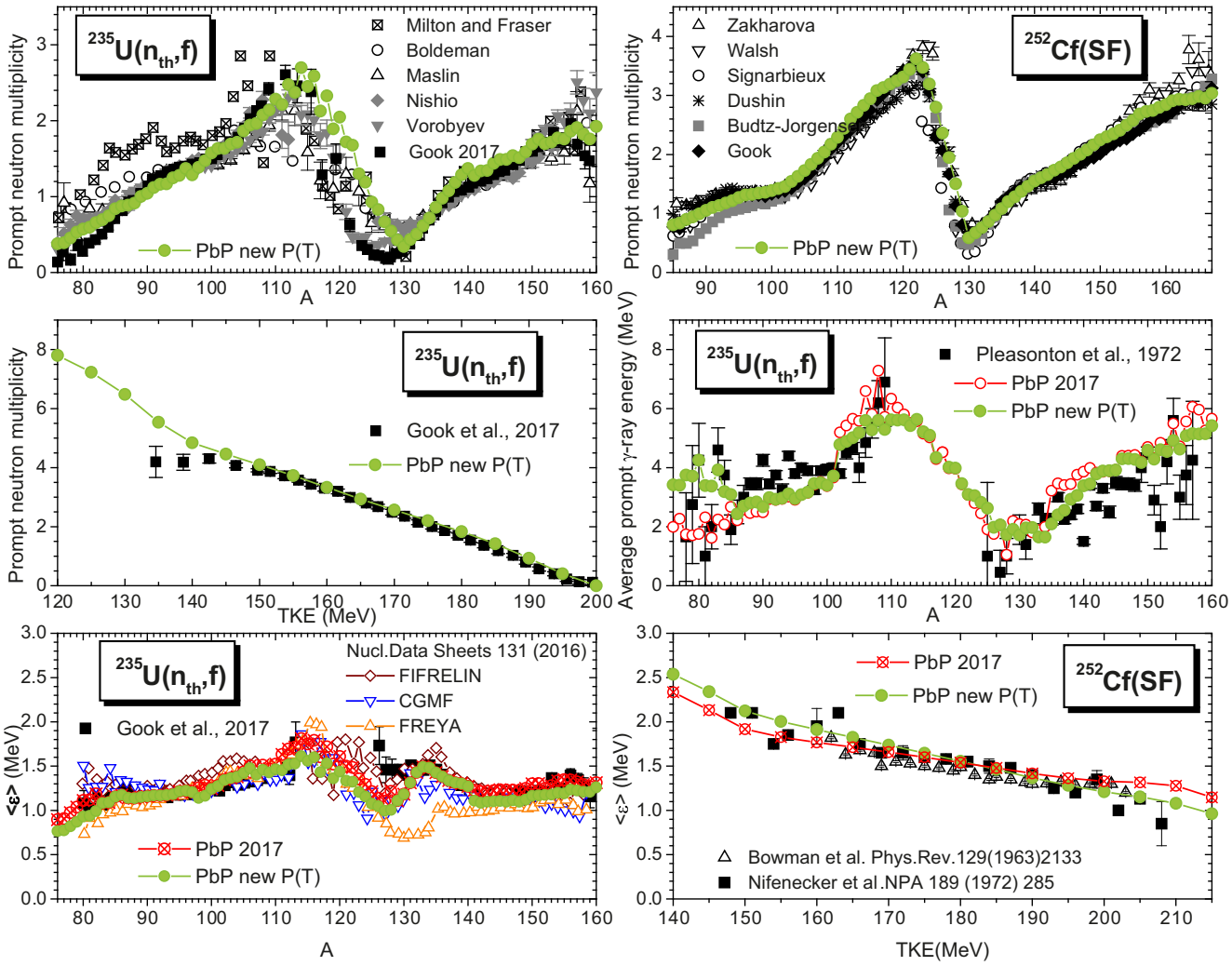

Fig. 27. Examples of PbP results obtained with the new form of $P(T)$ plotted with full green circles as follows: $\overline{\nu}(A)$ of ^{235}U(n$_{\rm th}$, f) and ^{252}Cf(SF) in the upper part, $\langle\nu\rangle$(TKE) and $E\gamma(A)$ of ^{235}U(n$_{\rm th}$, f) in the middle part, $\langle\varepsilon\rangle(A)$ of ^{235}U(n$_{\rm th}$, f) and $\langle\varepsilon\rangle$(TKE) of ^{252}Cf(SF) in the lower part, in comparison with the experimental data (different black and gray symbols), the PbP results from ref. [4] obtained with the $P(T)$ of Madland and Nix (red open circles or with a cross inside) and the results of the Monte Carlo codes FIFRELIN (open wine diamonds), CGMF (blue open down triangles) and FREYA (orange open up triangles) from ref. [3] (in the lower left part).

6 PbP model results using the new triangular form of P(T)

The triangular form of eq. (24) was included in the PbP treatment instead of the $P(T)$ form of Madland and Nix eq. (25) in order to see the differences in different prompt emission quantities.

The average prompt neutron multiplicity results $\overline{\nu}(A)$ and $\langle\nu\rangle$(TKE) obtained with the new $P(T)$ differ insignificantly from the results obtained with the $P(T)$ form of Madland and Nix. See as example the PbP results of $\overline{\nu}(A)$ and $\langle\nu\rangle$(TKE) plotted with full green circles in comparison with the experimental data (different black and gray symbols) in the upper part and the left middle part of fig. 27.

Visible differences between the PbP results obtained with $P(T)$ of eqs. (24) and (25) are expected in the case of average center-of-mass energy of prompt neutrons, *i.e.* $\langle\varepsilon\rangle$ obtained with $P(T)$ of eq. (24) is expected to be slightly lower than $\langle\varepsilon\rangle$ obtained with $P(T)$ of Madland and Nix. This fact is visible in the case of $\langle\varepsilon\rangle(A)$, exemplified in the lower left part of fig. 27 for ^{235}U(n$_{\rm th}$, f), where the PbP result with the new $P(T)$ plotted with full green symbols is compared to the PbP result of ref. [4] given with red circles with a cross inside and also with the results of the Monte Carlo codes FIFRELIN (open wine diamonds), CGMF (open blue down triangles) and FREYA (open orange up triangles) from ref. [3]. In the case of $\langle\varepsilon\rangle$(TKE), exemplified in the lower right part of fig. 27 for ^{252}Cf(SF), the change in the decreasing slope induced by the use of different $P(T)$ into the PbP model is visible.

The slight decrease of $\langle\varepsilon\rangle$ obtained with $P(T)$ of eq. (24) compared to $\langle\varepsilon\rangle$ obtained with $P(T)$ of Madland and Nix can be easily demonstrated in the case of a constant $\sigma_c(\varepsilon)$. In this case the prompt neutron spectrum in the center-of-mass frame of eq. (22) becomes

$$\Phi(\varepsilon) = \frac{2\varepsilon}{T_{\max}^2} E_1(\varepsilon/T_{\max}) \quad \text{with } E_1(z) = \int_z^\infty \frac{\exp(-x)}{x}\mathrm{d}x, \tag{26}$$

where the maximum temperature is $T_{\max} = T_i$ in the case of $P(T)$ of Madland and Nix and $T_{\max} = 0.9T_i$ for $P(T)$ of eq. (24). The moments of the distribution given by eq. (26) can be evaluated by interchanging the order of integration, which leads to

$$\langle\varepsilon^n\rangle = \int_0^\infty \varepsilon^n \Phi(\varepsilon)\mathrm{d}\varepsilon = \frac{2(n+1)!}{n+2} T_{\max}^n, \tag{27}$$

giving for the average center-of-mass energy $\langle\varepsilon\rangle = (4/3)T_{\max}$. Consequently $\langle\varepsilon\rangle$ obtained with $P(T)$ of eq. (24) is 0.9 from $\langle\varepsilon\rangle$ obtained with $P(T)$ of Madland and Nix.

Some differences between the average prompt γ-ray energy results obtained with $P(T)$ of eqs. (24) and (25) are also expected. An example of average $E\gamma$ as a function of A is illustrated in the middle right part of fig. 27 for $^{235}\mathrm{U}(\mathrm{n_{th}},\mathrm{f})$. The PbP result with the new $P(T)$ is plotted with full green circles in comparison with the previous result from ref. [4] (open red circles) obtained with $P(T)$ of Madland and Nix and the experimental data of Pleasonton *et al.* [37] (full black squares).

Note that the PbP results using $P(T)$ of eq. (24) given in fig. 27 were obtained with $\sigma_c(\varepsilon)$ provided by optical model calculations with the potential parameterization of Becchetti-Greenlees [15] and energy-dependent level density parameters of fragments of the super-fluid model with shell corrections of Möller and Nix [21] and the parameterizations of Ignatiuk [18] for the damping and the asymptotic level density parameter.

It is known that the shape of the prompt neutron spectrum (irrespective of the sequential or global treatment of successive prompt neutron emission) is sensitive to different prescriptions concerning $\sigma_c(\varepsilon)$ (see ref. [3] and references therein), the level density parameters of fragments and to the consideration or not of anisotropy. The triangular $P(T)$ form of Madland and Nix used in the Los Alamos model (*i.e.*, only one fragmentation taken into account with average model parameters) with equal maximum temperatures of the complementary light and heavy fragments as in ref. [1] or non-equal maximum temperatures of complementary fragments as in ref. [2] also impacts the prompt neutron spectrum [2,4]. The influence of the $P(T)$ form of eq. (24) on the shape of the prompt neutron spectrum in the center-of-mass and laboratory frames will be the subject of a future paper.

7 Conclusions

A deterministic treatment of the sequential emission of prompt neutrons based on successive equations of the residual temperature was developed. These equations, based on the assumption of fragment level densities in the Fermi gas regime, were solved under the approximations of non energy-dependent level density parameters of fragments and analytical expressions of the compound nucleus cross-sections of the inverse process of successive neutron evaporation from initial and residual fragments.

Because the main objective was the investigation of a possible systematic behaviour of the residual temperature distribution, this sequential emission treatment was applied to 11 nuclei undergoing fission spontaneously (^{252}Cf(SF), $^{236-244}$Pu(SF)), induced by thermal neutrons ($^{235}\mathrm{U}(\mathrm{n_{th}},\mathrm{f})$, $^{239}\mathrm{Pu}(\mathrm{n_{th}},\mathrm{f})$) and by fast neutrons with energies up to about 5 MeV ($^{237}\mathrm{Np}(\mathrm{n},\mathrm{f})$, $^{238,244}\mathrm{U}(\mathrm{n},\mathrm{f})$), for which reliable experimental fragment distributions exist.

This sequential emission modeling was validated by the good agreement of its results (*e.g.*, prompt neutron multiplicity $\overline{\nu}(A)$, $\langle\nu\rangle$(TKE), average prompt neutron energy $\langle\varepsilon\rangle(A)$, $\langle\varepsilon\rangle$(TKE), prompt γ-ray energy $\overline{E}_\gamma(A)$, prompt neutron multiplicity distribution $P(\nu)$, etc.) with the experimental data and the results of other prompt emission models (*e.g.*, PbP, FIFRELIN, etc.).

The shapes of all residual temperature distributions, corresponding to the light and heavy fragment groups and to all fragments, obtained from the present sequential emission calculations, can be well approximated by triangular forms with a moderately broad cut-off at high temperatures.

In order to use such triangular forms of the residual temperature distribution into prompt emission models with a global treatment of the sequential emission, a relation between the average residual temperature (first order momentum of $P(T)$) and the average temperature of initial fragments (before prompt neutron emission) is needed.

A very important finding is that for all studied fissioning nuclei, irrespective of the type of fission (spontaneous or induced by neutrons with energies from thermal up to the limit of the second chance fission threshold), the ratio of the average residual temperature to the average initial temperature is very close to 0.6. These average temperature ratios are referring to the light and heavy fragments groups and to all fragments. Moreover the use of different approximations concerning the level density parameters of fragments and the compound nucleus cross-section of the inverse process (even the rough approximation of a constant compound nucleus cross-section) leads to the same value ≈ 0.6 of the average residual to initial temperature ratio.

The expression of the first order momentum of the triangular $P(T)$ form as 0.6 from the temperature of initial fragments together with the replacement of the moderately broad cut-off at high temperatures by a sharp cut-off (*i.e.*, considering as upper limit of the residual temperature the value corresponding to the maximum of the triangular $P(T)$ form) gives a general simple form of $P(T)$ applicable to any fissioning system in the frame of prompt emission models with a global treatment of the sequential emission.

This proposed $P(T)$ form with the first order momentum $\langle T \rangle = 0.6T_i$ and the maximum temperature value $T_{\max} = 0.9T_i$, differing from the currently used form of Madland and Nix with $\langle T \rangle = (2/3)T_i$ and the maximum temperature value equal to the temperature of initial fragments can lead to an improvement of the very popular Los Alamos model and of the PbP model, too.

This work was done in the frame of the Romanian research project PN-III-P4-PCE-2016-0014.

References

1. D.G. Madland, J.R. Nix, Nucl. Sci. Eng. **81**, 213 (1982).
2. D.G. Madland, A.C. Kahler, Nucl. Phys. A **957**, 289 (2017).
3. R. Capote, Y.J. Chen, F.-J. Hambsch, N.V. Kornilov, J.P. Lestone, O. Litaize, B. Morillon, D. Neudecker, S. Oberstedt, T. Ohsawa, N. Otuka, V.G. Pronyaev, A. Saxena, O. Serot, O.A. Shcherbakov, N.C. Shu, D.L. Smith, P. Talou, A. Trkov, A.C. Tudora, R. Vogt, S. Vorobyev, Nucl. Data Sheets **131**, 1 (2016).
4. A. Tudora, F.-J. Hambsch, Eur. Phys. J. A. **53**, 159 (2017).
5. A. Al-Adili, F.-J. Hambsch, S. Pomp, S. Oberstedt, Phys. Rev. C **86**, 054601 (2012).
6. A. Göök, F.-J. Hambsch, M. Vidali, Phys. Rev. C **90**, 064611 (2014).
7. C. Wagemans, E. Allaert, A. Deruytter, R. Barthelemy, P. Schillebeeckx, Phys. Rev. C **30**, 218 (1984).
8. L. Demattè, *Investigation of the fission fragments mass and energy distributions of* ^{236,238,240,242,244}Pu(SF), PhD Thesis, Univ. of Ghent, coordinator C. Wagemans (1995-1996).
9. F.-J. Hambsch, F. Vivès, P. Siegler, S. Oberstedt, Nucl. Phys. A **679**, 3 (2000).
10. F. Vivès, F.-J. Hambsch, H. Bax, S. Oberstedt, Nucl. Phys. A **662**, 63 (2000).
11. A. Al-Adili, F.-J. Hambsch, S. Pomp, S. Oberstedt, Phys. Rev. C **93**, 034603 (2016).
12. A.C. Wahl, At. Data Nucl. Data Tables **39**, 1 (1988).
13. A. Tudora, F.-J. Hambsch, I. Visan, G. Giubega, Nucl. Phys. A **940**, 242 (2015).
14. C. Morariu, A. Tudora, F.-J. Hambsch, S. Oberstedt, C. Manailescu, J. Phys. G: Nucl. Part. Phys. **39**, 055103 (2012).
15. R. Capote, M. Herman, P. Oblozinsky, P.G. Young, S. Goriely, T. Belgya, A.V. Ignatiuk, A.J. Koning, S. Hilare, V.A. Plujko, M. Avrigeanu, O. Bersillon, M.B. Chadwick, T. Fukahory, Zhigang Ge, Yinlu Han, S. Kailas, J. Kopecky, V.M. Maslov, G. Reffo, M. Sin, E.Sh. Soukhovitskii, P. Talou, Nucl. Data Sheets **110**, 3107 (2009) IAEA-RIPL3 electronic library, available online at `https://www-nds.iaea.org`, segment IV, *Optical model parameters*, Becchetti-Greenlees, Koning-Delaroche.
16. O. Iwamoto, J. Nucl. Sci. Technol. **45**, 910 (2008).
17. R. Capote, M. Herman, P. Oblozinsky, P.G. Young, S. Goriely, T. Belgya, A.V. Ignatiuk, A.J. Koning, S. Hilare, V.A. Plujko, M. Avrigeanu, O. Bersillon, M.B. Chadwick, T. Fukahory, Zhigang Ge, Yinlu Han, S. Kailas, J. Kopecky, V.M. Maslov, G. Reffo, M. Sin, E.Sh. Soukhovitskii, P. Talou, Nucl. Data Sheets **110**, 3107 (2009) IAEA-RIPL3 electronic library, available online at `https://www-nds.iaea.org`, segment III, *Resonances* (the data file with s-wave resonances).
18. A.V. Ignatiuk, in IAEA-RIPL1-TECDOC-1034, Segment V (1998) Chapt. 5.1.4.
19. A. Gilbert, A.G.W. Cameron, Can. J. Phys. **43**, 1446 (1965).
20. T. von Egidy, D. Bucurescu, Phys. Rev. C **80**, 054310 (2009).
21. R. Capote, M. Herman, P. Oblozinsky, P.G. Young, S. Goriely, T. Belgya, A.V. Ignatiuk, A.J. Koning, S. Hilare, V.A. Plujko, M. Avrigeanu, O. Bersillon, M.B. Chadwick, T. Fukahory, Zhigang Ge, Yinlu Han, S. Kailas, J. Kopecky, V.M. Maslov, G. Reffo, M. Sin, E.Sh. Soukhovitskii, P. Talou, Nucl. Data Sheets **110**, 3107 (2009) IAEA-RIPL3 electronic library, available online at `https://www-nds.iaea.org`, segment I, *Nuclear masses and deformations*, database of Möller and Nix (FRDM).
22. J. Terrell, Phys. Rev. **113**, 527 (1959).
23. A. Tudora, F.-J. Hambsch, S. Oberstedt, G. Giubega, I. Visan, Nucl. Sci. Eng. **181**, 289 (2015).
24. C. Manailescu, A. Tudora, F.-J. Hambsch, C. Morariu, S. Oberstedt, Nucl. Phys. A **867**, 12 (2011).
25. I. Visan, G. Giubega, A. Tudora, Rom. Rep. Phys. **67**, 483 (2015).
26. K.-H. Schmidt, B. Jurado, C. Amoureux, C. Schmitt, Nucl. Data Sheets **131**, 107 (2016) GEF code version 2015/2.2, available online at `http://www.cenbg.in2p3.fr/-GEF-`; and `http://www.khs-erzhausen.de/GEF.html`.
27. A. Göök, F.-J. Hambsch, S. Oberstedt, EPJ Web of Conferences **146**, 04007 (2017).
28. R. Mueller, A.A. Naqvi, F. Käppeler, F. Dickmann, Phys. Rev. C **29**, 885 (1984) numerical data from EXFOR (available online at `https://www-nds.iaea.org`), entry 21834 (Mueller and Naqvi, 1981).
29. A. Tudora, F.-J. Hambsch, V. Tobosaru, Phys. Rev. C **94**, 044601 (2016).
30. A. Tudora, F.-J. Hambsch, V. Tobosaru, EPJ Web of Conferences **146**, 04004 (2017).
31. C. Manailescu, PhD Thesis University of Bucharest and CEA-Cadarache, France, coordinators O. Serot and A. Tudora (2012).
32. A. Göök, F.-J. Hambsch, S. Oberstedt, EPJ Web of Conferences **169**, 00004 (2018).
33. A. Tudora, F.-J. Hambsch, EPJ Web of Conferences **169**, 00025 (2018).
34. H. Nifenecker, C. Signarbieux, R. Babinet, J. Poitou, *Neutron and gamma emission in fission*, IAEA-SM-174/207 117 review paper (1973).
35. A. Tudora, F.-J. Hambsch, G. Giubega, I. Visan, Nucl. Phys. A **933**, 165 (2015).
36. A. Tudora, F.-J. Hambsch, Ann. Nucl. Energy **37**, 771 (2010).
37. F. Pleasonton, R.L. Ferguson, H.W. Schmitt, Phys. Rev. C **6**, 1023 (1972).